

Chemical On/Off Switching of Mechanically Planar Chirality and Chiral Anion Recognition in a [2]Rotaxane Molecular Shuttle

Stefano Corra,[†] Christiaan de Vet,[†] Jessica Groppi,[†] Marcello La Rosa,[†] Serena Silvi,[‡] Massimo Baroncini,^{*,†,§} and Alberto Credi^{*,†,§}

[†] CLAN-Center for Light Activated Nanostructures, Dipartimento di Scienze e Tecnologie Agro-alimentari, Università di Bologna, Via Gobetti 101, 40129 Bologna, Italy

[‡] Dipartimento di Chimica “G. Ciamician”, Università di Bologna, Via Selmi 2, 40126 Bologna, Italy

[§] Istituto ISOF-CNR, Via Gobetti 101, 40129 Bologna, Italy

E-mail: massimo.baroncini@unibo.it, alberto.credi@unibo.it

SUPPORTING INFORMATION

1. Materials and methods	S2
2. Synthesis of compounds $1\text{H}^{3+}\cdot 3\text{I}^-$ and $2\text{H}^{3+}\cdot 3\text{I}^-$	S3
3. Characterization of $1\text{H}^{3+}\cdot 3\text{I}^-$ and $2\text{H}^{3+}\cdot 3\text{I}^-$	S10
4. Dynamic NMR experiments	S15
5. Luminescence switching	S36
6. Circular dichroism	S36
7. Molecular modelling	S38
8. References	S39

1. Materials and methods

General materials. All reagents and chemicals were purchased from Sigma-Aldrich or VWR international and used as received unless otherwise stated. Anhydrous THF was prepared by distillation over LiAlH_4 under an argon atmosphere. Flash column chromatography was performed using Sigma Aldrich Silica 40 (230-400 mesh size or 40-63 μm) as the stationary phase. Size exclusion chromatography was performed using Biorad Biobeads SX-3 as the stationary phase. Thin layer chromatography was performed on TLC Silica gel 60 F254 coated aluminum plates from Merck.

NMR Spectroscopy. NMR spectra were recorded on an Agilent DD2 spectrometer operating at 500 MHz. Chemical shifts are quoted in ppm relative to tetramethylsilane using the residual solvent peak as a reference standard and all coupling constants (J) are expressed in Hertz (Hz). For variable temperature experiments, the low temperatures were calibrated using a neat methanol sample. The shuttling rates were calculated from the line shape analysis of the NMR spectra using the program TOPSPIN 3.5.

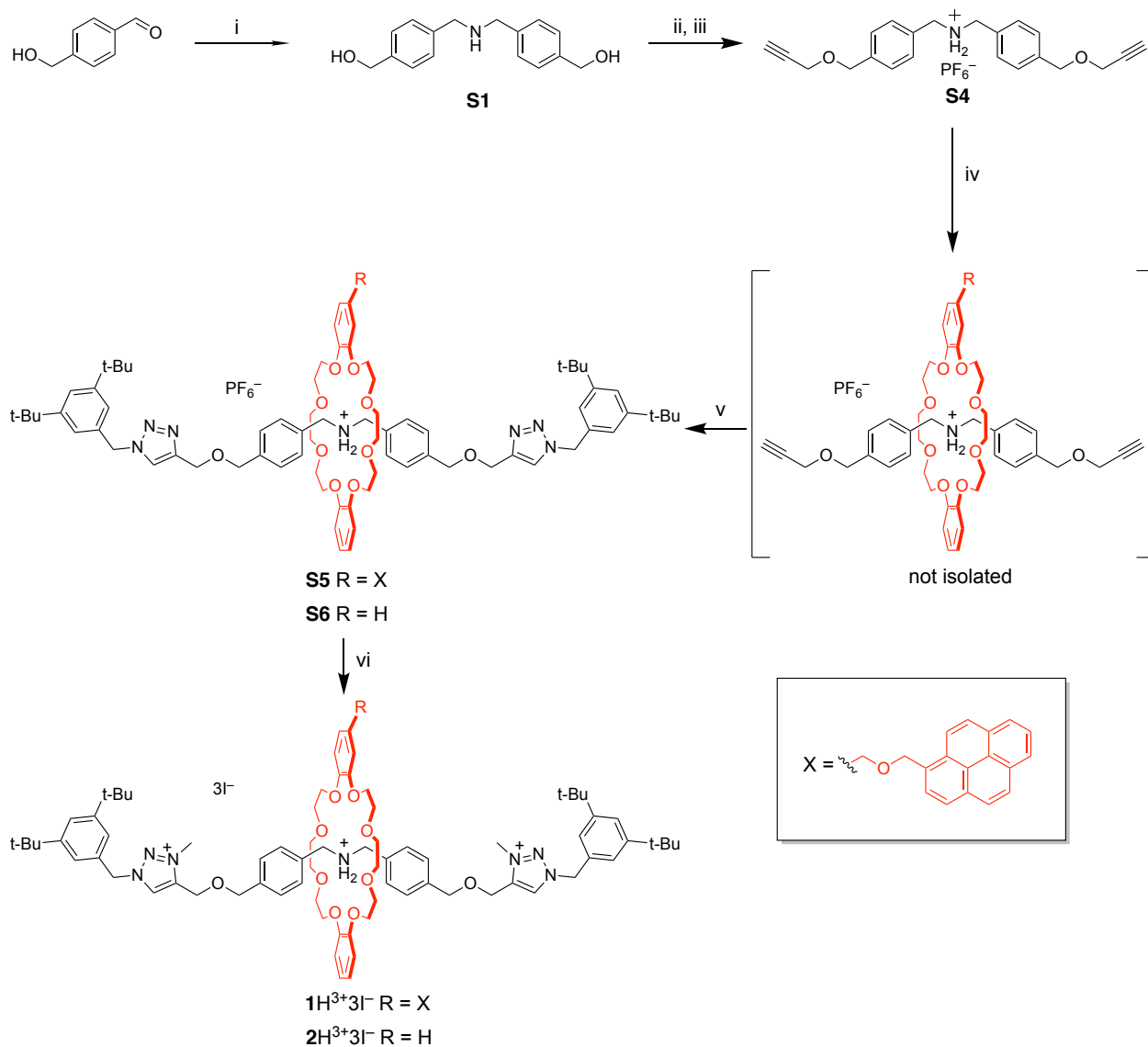
Mass spectrometry. Low resolution mass spectrometry (LRMS) measurements were performed on a Thermo Fischer Quantum Access Mass instrument equipped with an ESI source and a triple quadrupole ion analyzer.

UV-Visible absorption and luminescence spectroscopy. Electronic absorption spectra in the 250-800 nm range were recorded on a Perkin-Elmer Lambda 750 spectrophotometer. The experimental error on the wavelength values was ± 1 nm. Luminescence emission spectra in the 350-700 nm range were recorded with a FLS-920 Edinburgh spectrofluorimeter. The experimental error on the wavelength values was ± 1 nm. All the experiments were carried out at room temperature in a 1 cm quartz cuvette.

Circular dichroism spectroscopy. Circular dichroism spectra in the range 250-500 nm were recorded on a Jasco-175 spectropolarimeter. Instrumental parameters were set as: data pitch 1 nm, band width 2 nm, response 0.5 s, sensitivity standard, and scan speed 100 nm min^{-1} . All the experiments were carried out at room temperature in a 1 cm quartz cuvette.

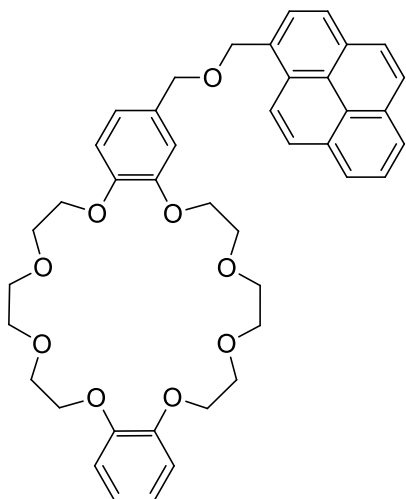
2. Synthesis of compounds $1\text{H}^{3+}\cdot 3\text{I}^-$ and $2\text{H}^{3+}\cdot 3\text{I}^-$

4-(hydroxymethyl)benzaldehyde, 3,5-di-(*tert*-butyl)benzyl azide, and 2-hydroxymethyl-dibenzo-24-crown-8 were synthesized according to previously published procedures.¹⁻³



Scheme S1. Synthetic route towards compounds $1\text{H}^{3+}\cdot 3\text{I}^-$ and $2\text{H}^{3+}\cdot 3\text{I}^-$. i) HMDS, LiClO₄, NaBH₄, MeOH. ii) Boc₂O, MeOH, ultrasound iii) NaH, Propargyl bromide, THF; CF₃CO₂H/CH₂Cl₂ (1:1), NH₄PF₆, acetone. iv) DB24C8Pyr (for $1\text{H}^{3+}\cdot 3\text{I}^-$) or DB24C8 (for $2\text{H}^{3+}\cdot 3\text{I}^-$), CH₂Cl₂. v) Cu(CH₃CN)PF₆, 3,5-di-(*tert*-butyl)benzyl azide, CH₂Cl₂. vi) CH₃I.

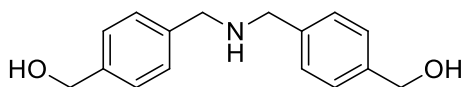
1-(2-Methoxymethyl-dibenzo-24-crown-8)pyrene (DB24C8Pyr)



To a solution of 2-hydroxymethyl-dibenzo-24-crown-8 (466 mg, 0.97 mmol) in anhydrous THF (30 mL), NaH (140 mg, 5.8 mmol) was added under a nitrogen atmosphere. Then, a suspension of 1-(bromomethyl)pyrene (345 mg, 1.17 mmol) in 40 mL of anhydrous THF was added dropwise. The reaction mixture was heated to 80 °C and stirred for 8 hours. Afterwards, the reaction mixture was cooled down to room temperature, H₂O (10 mL) was added and volatiles were removed under reduced pressure. The residue was partitioned in CHCl₃/H₂O (1:1). The aqueous layer was extracted with CHCl₃ and the combined organic layers were washed with

water, dried over Na₂SO₄, and concentrated under vacuum. The crude product was purified by flash chromatography (SiO₂, CH₂Cl₂/MeOH 98:2) and recrystallized from CH₂Cl₂/hexane to yield the title compound as pale yellow crystals (345 mg, 0.48 mmol, 49%). **¹H-NMR (500 MHz, CD₃CN, 298 K):** δ (ppm) 8.38 (d, *J* = 9.3 Hz, 1H, ArH), 8.29-8.24 (m, 2H, ArH), 8.21 (d, *J* = 7.8 Hz), 1H, ArH), 8.19 (d, *J* = 9.3 Hz, 1H, ArH), 8.12 (s, 2H, ArH), 8.07 (d, *J* = 7.8 Hz, 1H, ArH), 8.05 (t, *J* = 7.8 Hz, 1H, ArH), 6.95-6.82 (m, 7H, ArH), 5.22 (s, 2H, CH₂), 4.59 (s, 2H, CH₂), 4.10-4.02 (m, 6H, CH₂), 4.01-3.95 (s, 2H, CH₂), 3.81-3.73 (m, 6H, CH₂), 3.72-3.68 (m, 2H, CH₂), 3.66 (s, 4H, CH₂), 3.65-3.59 (m, 4H, CH₂). **¹³C-NMR (125 MHz, CD₃CN, 298 K):** δ (ppm) 149.9, 149.7, 149.3, 133.3, 132.7, 132.3, 132.2, 131.8, 128.6, 128.5, 128.4, 128.4, 127.3, 126.3, 125.6, 124.9, 122.3, 121.9, 115.6, 114.4, 114.6, 72.9, 71.7, 71.3, 70.6, 70.5, 69.9, 69.8, 69.7. **LRMS (ESI⁺)** *m/z* calculated for C₄₂H₄₄NaO₉⁺ [M+Na]⁺ 715.3; found: 714.9.

Bis(4-(hydroxymethyl)benzyl)amine (S1)

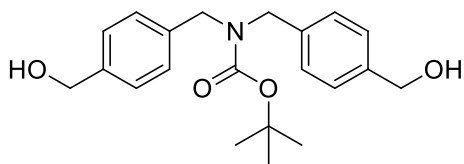


(4-hydroxymethyl)benzaldehyde (1.5 g, 11 mmol) and LiClO₄ (1.7 g, 16 mmol) were suspended in hexamethyldisilazane (HMDS) (5 mL). The suspension

was heated at 65°C for 2.5 hours. The resulting thick paste was dissolved in anhydrous MeOH (30 ml) and cooled at 0°C with an ice bath. NaBH₄ (778 mg, 22 mmol) was added in portions over 10 min and the solution was stirred for further 2 hours at 0°C. MeOH was removed under reduced pressure, the residue was suspended in aqueous NaHCO₃ (sat. 80 mL) and stirred for 30 min. The water layer was extracted with EtOAc (3x40 mL) and the combined organic layers were washed with brine (1x30 mL), dried over Na₂SO₄ and concentrated under vacuum. The resulting oil (1.2 g, 4.73 mmol, 86%) was used without further purification. **¹H-NMR (500 MHz, DMSO-d₆, 298 K):** δ (ppm) 7.32-7.24 (m, 8H, ArH), 5.10 (t, *J* = 5.3 Hz, 2H, OH), 4.49 (s, 4H, CH₂), 3.66 (s, 4H, CH₂). **¹³C-NMR (125 MHz, DMSO-d₆, 298 K):** δ (ppm) 140.8, 138.9, 127.7,

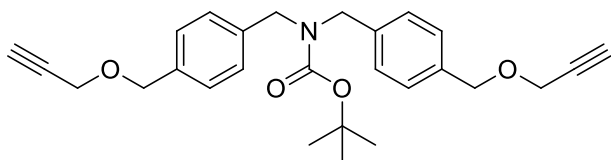
126.4, 62.8, 51.8.

Tert-butyl bis(4-(hydroxymethyl)benzyl)carbamate (**S2**)



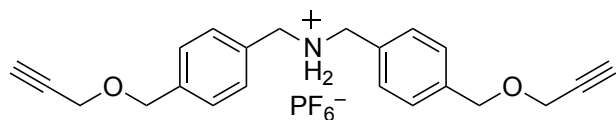
Di-*tert*-butyl dicarbonate (1.16 g, 5.32 mmol) was added to a solution of **S1** (1.14 g, 4.43 mmol) in MeOH (15 mL) and the reaction mixture was sonicated for 10 min. The solvent was evaporated and the crude product was purified by flash chromatography (SiO₂, hexane/EtOAc 40:60) to yield the title compound **S2** (1.29 g, 3.61 mmol, 82%). ¹H-NMR (500 MHz, DMSO-d₆, 298 K): δ (ppm) 7.29 (d, *J* = 7.4 Hz, 4H, ArH), 7.17 (br, 4H, ArH), 5.14 (t, *J* = 5.3 Hz, 2H, OH), 4.47 (d, *J* = 4.4 Hz, 4H, CH₂), 4.29 (br, 4H, CH₂), 1.40 (s, 9H, CH₃). Analysis is in line with previously published data.⁴

Tert-butyl bis(4-((prop-2-yn-1-yloxy)methyl)benzyl)carbamate (**S3**)



A solution of **S2** (1.29 g, 3.62 mmol) in anhydrous THF (25 mL) was added dropwise to a suspension of NaH (522 mg, 21.7 mmol) in THF (15 mL) at 0°C under argon. The suspension was stirred for 30 min at 0°C. Propargyl bromide (80 % m/v in toluene, 1.8 mL, 18.1 mmol) was added dropwise, and stirring continued overnight. Volatiles were removed under reduced pressure and the residue extracted with EtOAc. The combined organic layers were washed with brine, dried over Na₂SO₄, and concentrated under vacuum. The crude product was purified by flash chromatography (SiO₂, hexane/EtOAc 80:20) to yield **S3** as a pale yellow oil (1.19 g, 2.74 mmol, 76%). ¹H-NMR (500 MHz, CDCl₃, 298 K): δ (ppm) 7.31 (d, *J* = 7.4 Hz, 4H, ArH), 7.19 (br, 4H, ArH), 4.6 (s, 4H, CH₂), 4.36 (br, 4H, CH₂), 4.18 (s, 4H, CH₂), 2.47 (s, 2H, CH), 1.49 (s, 9H, CH₃). ¹³C-NMR (125 MHz, CDCl₃, 298 K): δ (ppm) 156.1, 137.8, 136.4, 128.5, 128.3, 127.6, 80.3, 79.7, 74.8, 71.4, 57.2, 49.1, 48.8, 28.6.

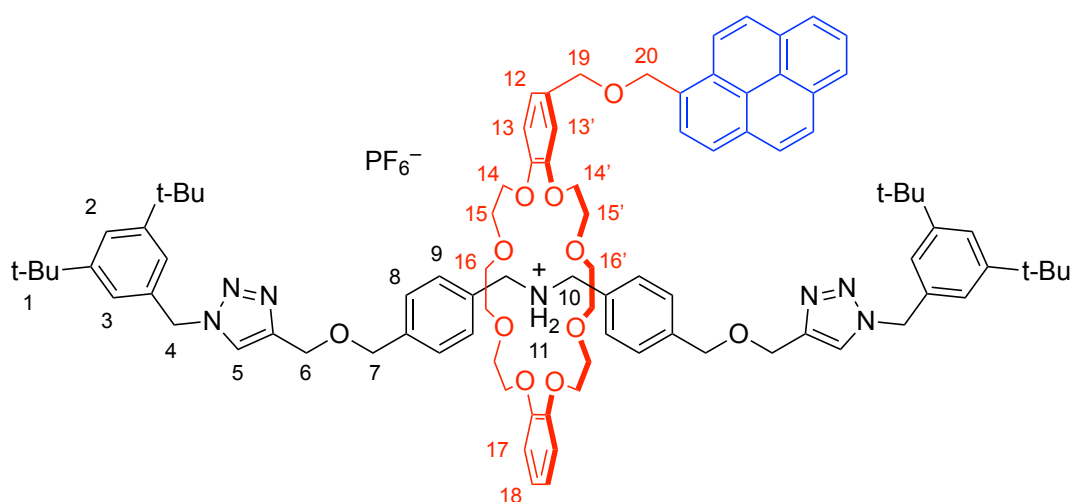
Bis(4-((prop-2-yn-1-yloxy)methyl)benzyl)ammonium hexafluorophosphate (**S4**)



S3 (800 mg, 1.83 mmol) was dissolved in CF₃CO₂H/CH₂Cl₂ (1:1, 24 mL) and stirred at room temperature for two hours. The resulting mixture was diluted with CH₂Cl₂ (15 mL) and washed with aqueous NaOH (2M, 20 mL). The organic layer was washed with water, brine, dried over Na₂SO₄, and concentrated. The resulting oil (630 mg, 1.89 mmol) was dissolved in the minimum amount of CH₃CN, and aqueous concentrated HCl was added dropwise. The precipitate was isolated, triturated with diethylether, and dispersed in acetone/CH₂Cl₂ (40 mL, 1:1). An aqueous saturated solution of NH₄PF₆ was added (20 mL), and the mixture was vigorously stirred overnight. The aqueous layer was

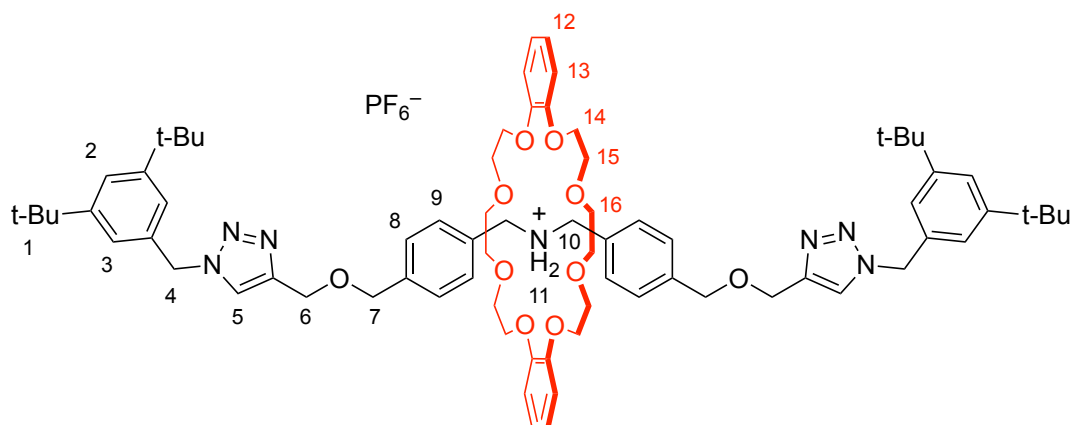
extracted with CH_2Cl_2 and the combined organic layers were washed with water, dried over Na_2SO_4 , and concentrated to yield **S4** (540 mg, 1.13 mmol, 60%). **$^1\text{H-NMR}$ (500 MHz, CD_3CN , 298 K):** δ (ppm) 7.46 (d, $J = 8.1$ Hz, 4H, ArH), 7.43 (d, $J = 8.1$ Hz, 4H, ArH), 4.59 (s, 4H, CH_2), 4.23 (s, 4H, CH_2), 4.20 (d, $J = 1.9$ Hz, 4H, CH_2), 2.57 (t, $J = 2.2$ Hz, 2H, Alkyne CH). **$^{13}\text{C-NMR}$ (125 MHz, CD_3CN , 298 K):** δ (ppm) 140.7, 131.2, 130.6, 129.3, 80.6, 75.9, 71.6, 58.1, 52.1.

Asymmetric triazole rotaxane **S5-PF₆⁻**



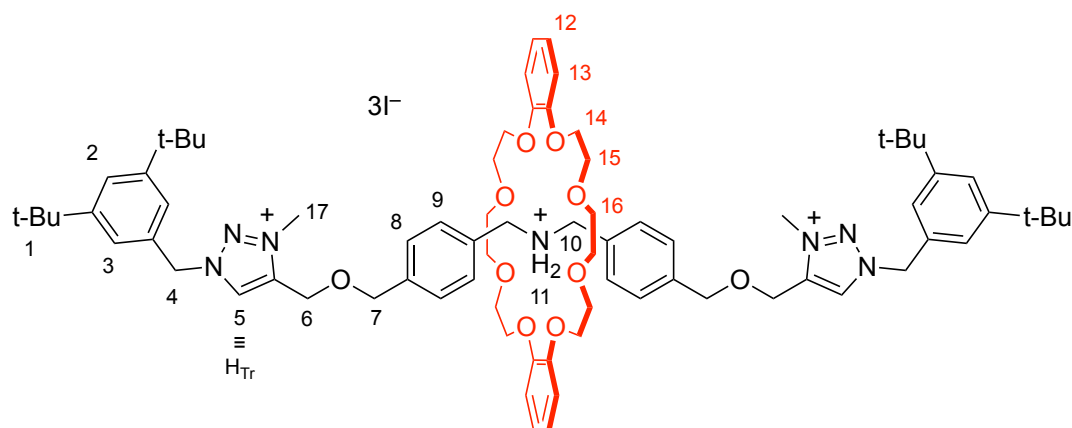
S4 (47 mg, 0.097 mmol) and **DB24C8Pyr** (336 mg, 0.49 mmol) were dissolved in degassed CH_2Cl_2 (10 mL) and stirred for 3 hours under a nitrogen atmosphere. 3,5-di-(*tert*-butyl)benzyl azide (60 mg, 0.24 mmol) and $\text{Cu}(\text{CH}_3\text{CN})_4\text{PF}_6$ (80 mg, 0.21 mmol) were added and stirring continued overnight. The mixture was diluted with CH_2Cl_2 , washed with an aqueous solution of EDTA (0.1 M), and water. The organic layer was dried over Na_2SO_4 and concentrated under vacuum. The crude product was purified by size exclusion chromatography (Biobeads SX-3, CHCl_3) to yield **S5** as a yellow glassy solid (81 mg, 50%). **$^1\text{H-NMR}$ (500 MHz, CDCl_3 , 298 K):** δ (ppm) 8.36 (d, $J = 9.1$ Hz, H_{pyrene}), 8.19-8.14 (m, 2H, H_{pyrene}), 8.14-8.08 (m, 2H, H_{pyrene}), 8.03 (s, 2H, H_{pyrene}), 8.01-7.95 (m, 2H, H_{pyrene}), 7.54 (br, overlap of peaks, 2H, $\text{H}_{5/11}$), 7.37 (t, $J = 1.7$ Hz, H_2), 7.19 (d, 7.8 Hz, 4H, H_9), 7.15 (d, $J = 7.8$ Hz, 4H, H_8), 7.12 (s, 4H, H_3), 6.86-6.77 (m, 3H, $\text{H}_{12/13/13'}$), 6.74-6.65 (m, 4H, $\text{H}_{17/18}$), 5.46 (s, 4H, H_4), 5.22 (s, 2H, H_{19}), 4.57-4.50 (m, peaks overlap, 6H, $\text{H}_{6/20}$), 4.46 (t, $J = 6.5$ Hz, H_{10}), 4.41 (s, 4H, H_7), 4.07-3.98 (m, 6H, H_{14}), 3.92-3.86 (m, 2H, $\text{H}_{14'}$), 3.74-3.64 (m, 6H, H_{15}), 3.57-3.51 (m, 2H, $\text{H}_{15'}$), 3.41-3.33 (m, 6H, H_{16}), 3.33-3.26 (m, 2H, $\text{H}_{16'}$), 1.26 (s, 36H, H_1). **$^{13}\text{C-NMR}$ (125 MHz, CDCl_3 , 298 K):** δ (ppm) 151.9 (C_{Ar} , quaternary), 147.6/147.5/145.1 (C_{crown} , quaternary), 145.0 (C_{Ar} , quaternary), 139.5 (C_{Ar} , quaternary), 134.0 (C_{Ar} , quaternary), 132.2 (C_{crown} , quaternary), 131.6 (C_{pyrene} , quaternary), 131.4 (C_{pyrene} , quaternary), 131.0 (C_{pyrene} , quaternary), 130.9 (C_{Ar} , quaternary), 129.7 (C_{pyrene} , quaternary), 129.4 (C_9), 128.0 (C_8), 127.9 (C_{pyrene}), 127.7 (C_{pyrene}), 127.6 (C_{pyrene}), 127.6 (C_{pyrene}), 126.2 (C_{pyrene}), 126.1 (C_{pyrene}), 125.1 (C_{pyrene} , quaternary), 124.9 (C_{pyrene} , quaternary), 124.7 (C_{pyrene}), 123.8 (C_{pyrene}), 123.1 (C_5), 122.9 (C_2), 122.7 (C_3), 121.9 (C_{18}), 121.3 (C_{12}), 113.0 (C_{17}), 112.9 (C_{13}), 112.7 ($\text{C}_{13'}$), 71.8 (C_{19}), 71.6 (C_7), 71.1 (C_{20}), 70.8 (C_{14}),

Symmetric triazole rotaxane **S6**·PF₆⁻



S4 (75 mg, 0.16 mmol) and dibenzo-24-crown-8-ether (351 mg, 0.78 mmol) were dissolved in degassed CH₂Cl₂ (12 mL) and stirred for 3 hours under a nitrogen atmosphere. 3,5-di-*tert*-butylbenzyl azide (60 mg, 0.24 mmol) and Cu(CH₃CN)₄PF₆ (80 mg, 0.21 mmol) were added and stirring continued overnight. The mixture was diluted with CH₂Cl₂, washed with an aqueous solution of EDTA (0.1 M), and water. The organic layer was dried over Na₂SO₄ and concentrated under vacuum. The crude product was purified by size exclusion chromatography (Biobeads SX-3, CHCl₃) to yield **S6** as a colourless glassy solid (107 mg, 0.075 mmol, 47%). **¹H-NMR (500 MHz, CDCl₃, 298 K):** δ (ppm) 7.59 (s, 2H, H₅), 7.37 (t, J = 1.7 Hz, 2H, H₂), 7.24 (d, overlapping with solvent peak, 4H, H₈), 7.18 (d, J = 8.2 Hz, 4H, H₉), 7.14 (s, 4H, H₃), 6.85-6.79 (m, 4H, H₁₂), 6.77-6.71 (m, 4H, H₁₃), 5.50 (s, 4H, H₄), 4.85 (s, 4H, H₆), 4.52 (t, J = 6.2 Hz, 4H, H₁₀), 4.47 (s, 4H, H₇), 4.11-4.03 (m, 8H, H₁₄), 3.76-3.69 (m, 8H, H₁₅), 3.40 (s, 8H, H₁₆), 1.27 (s, 36H, H₁). **¹³C-NMR (125 MHz, CDCl₃, 298 K):** δ (ppm) 151.8 (C_{Ar}, quaternary), 147.5 (C_{crown}, quaternary), 145.0 (C_{Ar}, quaternary), 139.4 (C_{Ar}, quaternary), 134.0 (C_{Ar}, quaternary), 130.9 (C_{Ar}, quaternary), 129.3 (C₉), 128.0 (C₈), 123.0 (C₅), 122.8 (C₂), 122.7 (C₃), 121.9 (C₁₂), 112.9 (C₁₃), 71.5 (C₇), 70.8 (C₁₄), 70.3 (C₁₅), 68.4 (C₁₆), 63.7 (C₆), 54.9 (C₄), 52.5 (C₁₀), 35.0 (C, quaternary), 31.5 (C₁).

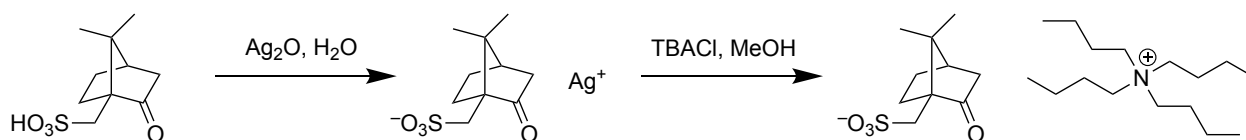
Symmetric rotaxane **2H**³⁺·3I⁻



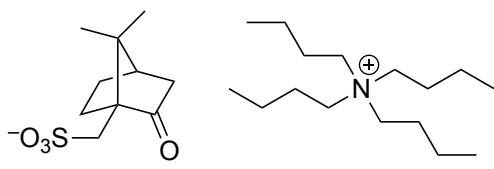
S6 (107 mg, 0.075 mmol) was dissolved in CH₃I (4 mL) and stirred at room temperature for 3
S8

days under a nitrogen atmosphere. The solution was concentrated under reduced pressure, the residue was dissolved in the minimum amount of CH_2Cl_2 and dispersed in diethylether (200 mL). The suspension was centrifuged at 3000 rpm for 5 min and the supernatant was removed to yield $2\text{H}^{3+}\cdot 3\text{I}^-$ as a pale yellow solid (110 mg, 0.066 mmol, 89%). **$^1\text{H-NMR}$ (500 MHz, CDCl_3 , 298 K):** δ (ppm) 9.11 (s, 2H, H_5), 7.63 (br, 2H, H_{11}), 7.45 (s, 2H, H_2), 7.39 (s, 4H, H_3), 7.32-7.25 (m, 8H, H_8/H_9), 6.86-6.81 (m, 4H, H_{12}), 6.81-6.76 (m, 4H, H_{13}), 5.78 (s, 4H, H_6), 4.83 (s, 4H, H_4), 4.62 (s, 4H, H_7), 4.53 (t, $J = 6.3$ Hz, 4H, H_{10}), 4.37 (s, 6H, H_{17}), 4.12-4.07 (m, 8H, H_{14}), 3.77-3.73 (m, 8H, H_{15}), 3.43 (s, 8H, H_{16}), 1.30 (s, 36H, H_1). **$^{13}\text{C-NMR}$ (125 MHz, CDCl_3 , 298 K):** δ (ppm) 152.6 (C_{Ar} , quaternary), 147.6 (C_{crown} , quaternary), 140.6 (C_{Ar} , quaternary), 137.7 (C_{Ar} , quaternary), 131.7 (C_{Ar} , quaternary), 130.4 (C_5), 130.1 (C_{Ar} , quaternary), 129.8 (C_9), 128.6 (C_8), 124.4 (C_2), 124.2 (C_3), 122.0 (C_{12}), 113.2 (C_{13}), 72.9 (C_7), 70.9 (C_{14}), 70.4 (C_{15}), 68.6 (C_{16}), 59.8 (C_6), 58.4 (C_4), 52.5 (C_{10}), 39.8 (C_{17}), 35.2 (C , quaternary), 31.6 (C_1). **LRMS (ESI+)** m/z calculated for $\text{C}_{78}\text{H}_{108}\text{N}_7\text{O}_{10}^{3+}$ $[\text{M}]^{3+}$ 434.3; found: 434.2, calculated for $\text{C}_{78}\text{H}_{107}\text{N}_7\text{O}_{10}^{2+}$ $[\text{M-H}]^{2+}$ 650.9; found: 650.8.

Tetrabutylammonium 1S-(+)-camphorsulfonate

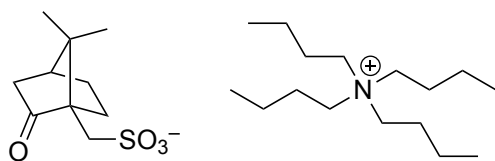


Scheme S2. Synthetic route towards Tetrabutylammonium 1S-(+)-camphorsulfonate



1S-(+)-camphorsulfonic acid (400 mg, 1.7 mmol) was dissolved in water (5 mL) and Ag_2O was added until precipitation was observed. The solution was filtered and the filtrate slowly added into a methanolic solution of tetrabutylammonium chloride (526 mg, 1.9 mmol, 30 mL). Precipitation of AgCl was immediately observed and stirring was continued for further 30 min. The solvent was removed under vacuum. The residue was partitioned in $\text{CH}_2\text{Cl}_2/\text{H}_2\text{O}$ (1:1) and the organic layer was washed with water (1 x 50 mL), dried over MgSO_4 and the solvent removed under vacuum. The crude product was recrystallized from ethyl acetate to yield the title compound as colourless needles (492 mg, 61%). **$^1\text{H NMR}$ (500 MHz, CDCl_3 , 298 K):** δ (ppm) 3.37 – 3.26 (m, 8H), 2.85 (td, $J = 13.0, 12.2, 3.2$ Hz, 1H), 2.79 (d, $J = 14.7$ Hz, 1H), 2.29 (dt, $J = 18.1, 4.0$ Hz, 1H), 2.08 – 1.90 (m, 5H), 1.84 (d, $J = 18.1$ Hz, 1H), 1.71 (d, $J = 4.8$ Hz, 1H), 1.70 – 1.60 (m, 8H), 1.45 (h, $J = 7.4$ Hz, 8H), 1.36 – 1.25 (m, 1H), 1.14 (s, 3H), 1.00 (t, $J = 7.3$ Hz, 12H), 0.82 (s, 3H). Analysis is in line with previously reported data.⁵

Tetrabutylammonium 1*R*-(-)-camphorsulfonate



The same procedure adopted for 1*S*-(+)-camphorsulfonate was followed to prepare tetrabutylammonium 1*R*-(-)-camphorsulfonate starting from 1*R*-(-)-camphorsulfonic acid (400 mg, 1.7 mmol) to yield 453 mg, 56% of product as colourless needles. ¹H NMR (500 MHz, CDCl₃, 298 K): δ (ppm) 3.41 – 3.24 (m, 8H), 2.89 – 2.73 (m, 1H), 2.29 (dt, *J* = 18.1, 4.0 Hz, 1H), 2.05 – 1.94 (m, 8H), 1.84 (d, *J* = 18.1 Hz, 1H), 1.66 (ddd, *J* = 15.6, 10.0, 6.2 Hz, 8H), 1.45 (h, *J* = 7.4 Hz, 8H), 1.32 (ddd, *J* = 11.4, 9.3, 3.7 Hz, 1H), 1.13 (s, 3H), 1.00 (t, *J* = 7.3 Hz, 12H), 0.82 (s, 3H). Analysis is in line with previously reported data.⁵

3. Characterization of 1H³⁺·3I⁻ and 2H³⁺·3I⁻

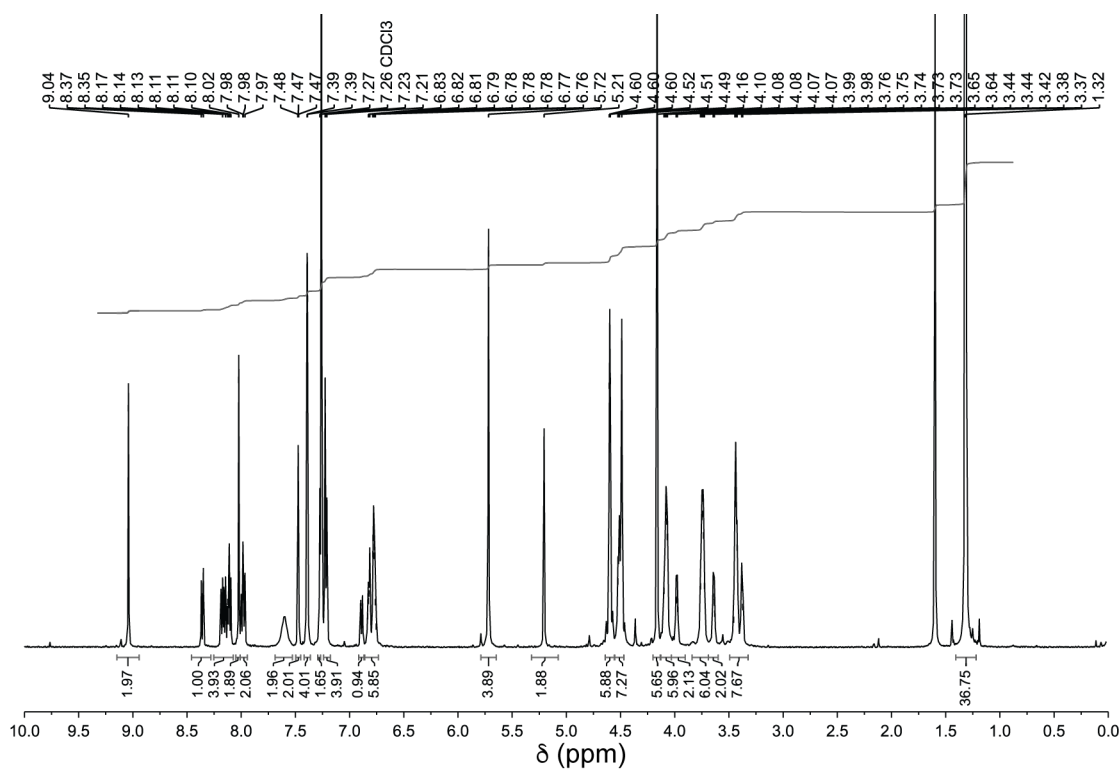


Figure S1. ¹H NMR spectrum of 1H³⁺·3I⁻ (500 MHz, CDCl₃, 298 K).

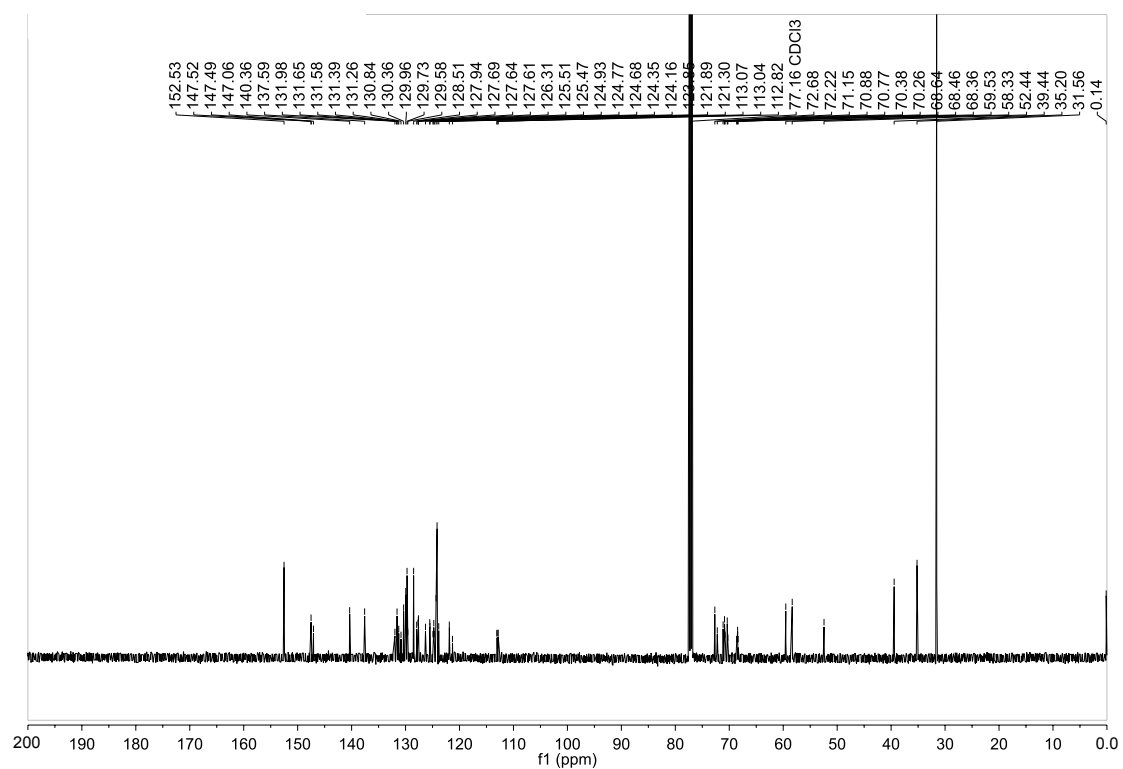


Figure S2. ^{13}C NMR spectrum of $1\text{H}^{3+}\cdot 3\text{I}^-$ (125 MHz, CDCl_3 , 298 K).

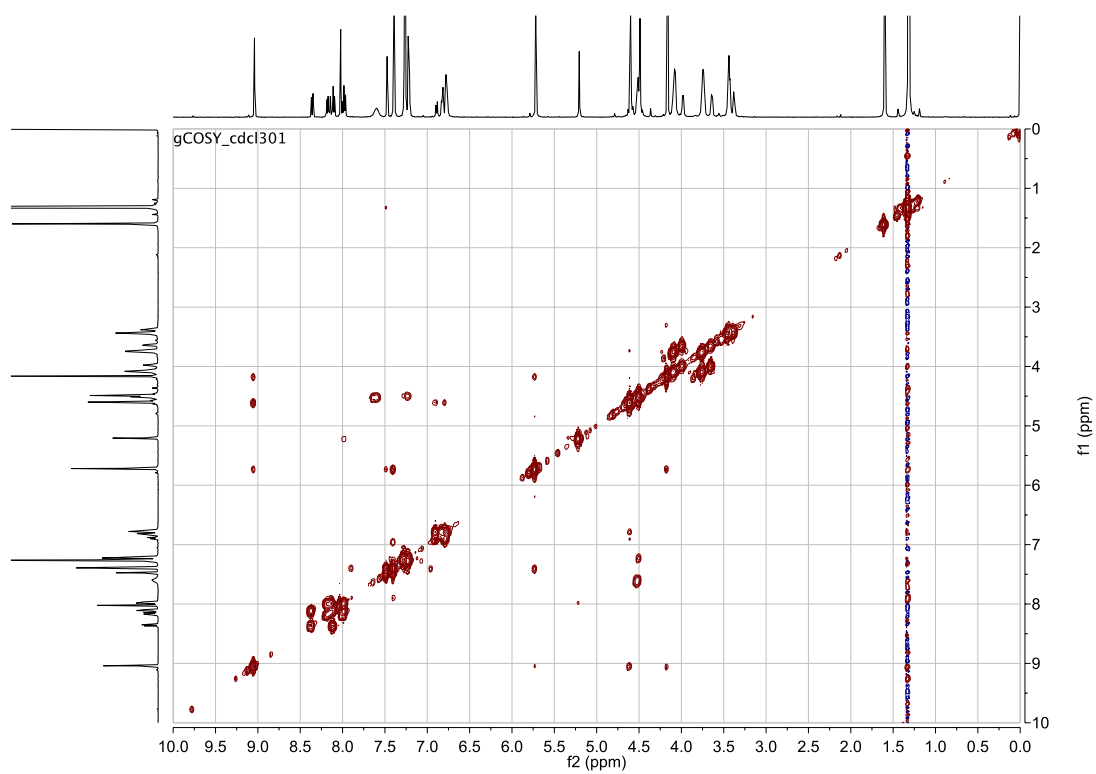


Figure S3. ^1H - ^1H COSY spectrum of $1\text{H}^{3+}\cdot 3\text{I}^-$ (500 MHz, CDCl_3 , 298 K).

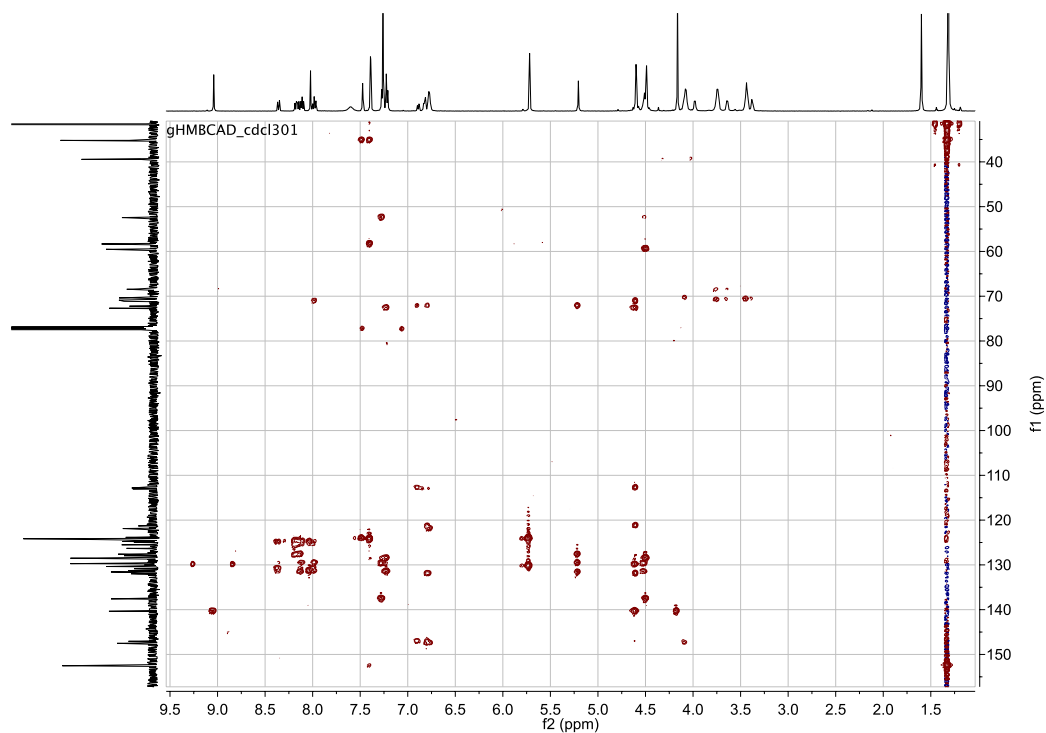


Figure S4. ^1H - ^{13}C HMBC spectrum of $1\text{H}^{3+}\cdot 3\text{I}^-$ (CDCl_3 , 298 K).

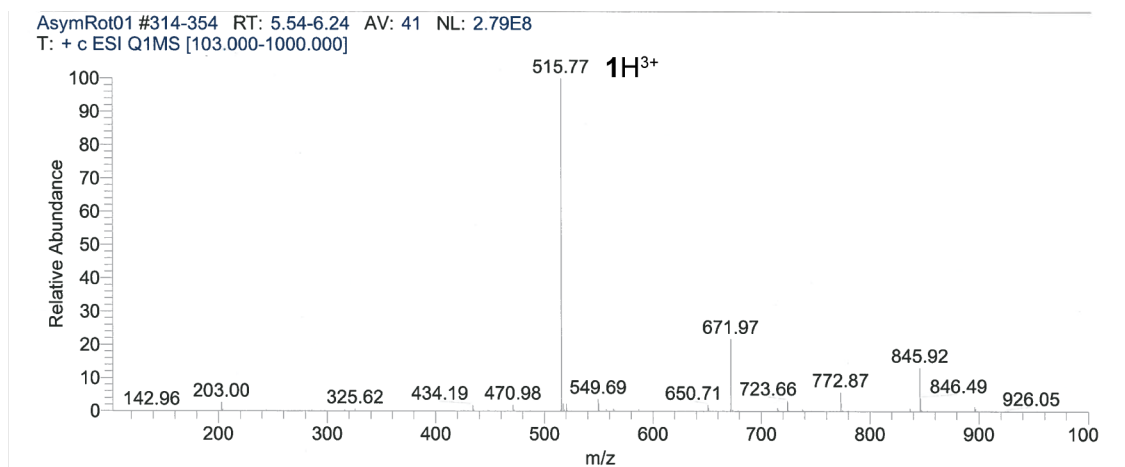


Figure S5. ESI-MS spectrum of $1\text{H}^{3+}\cdot 3\text{I}^-$.

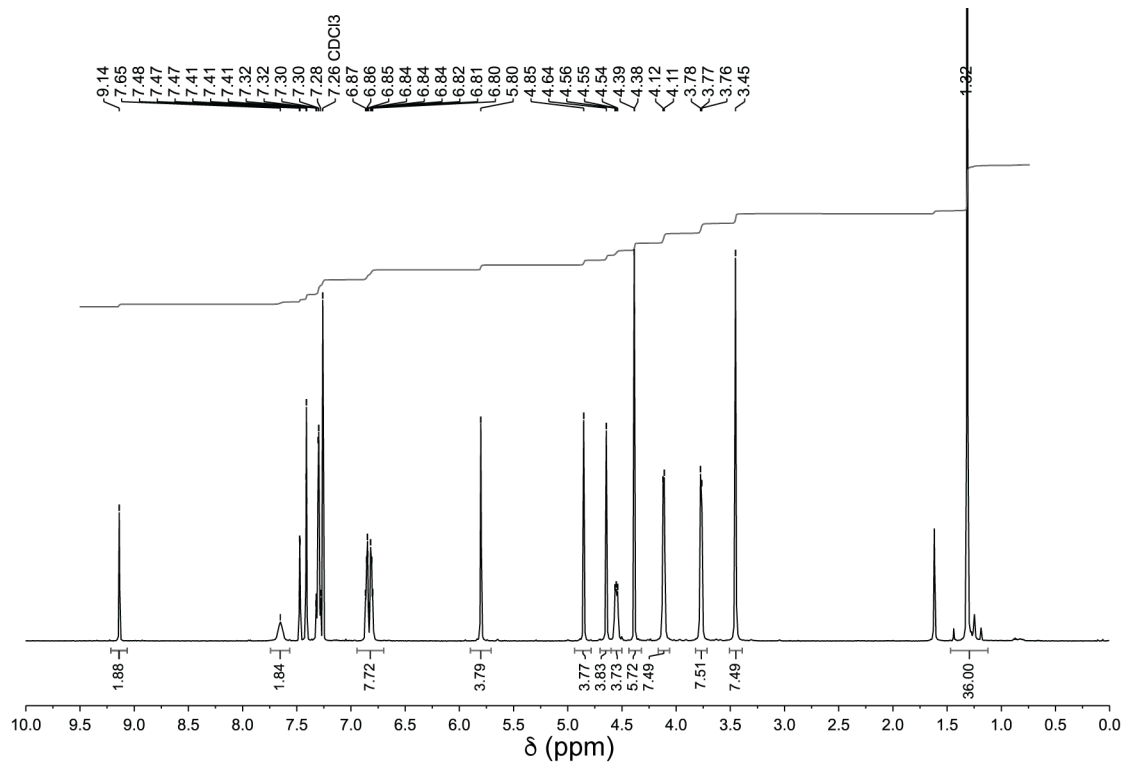


Figure S6. ^1H NMR spectrum of $2\text{H}^{3+}\cdot 3\text{I}^-$ (500 MHz, CDCl_3 , 298 K).

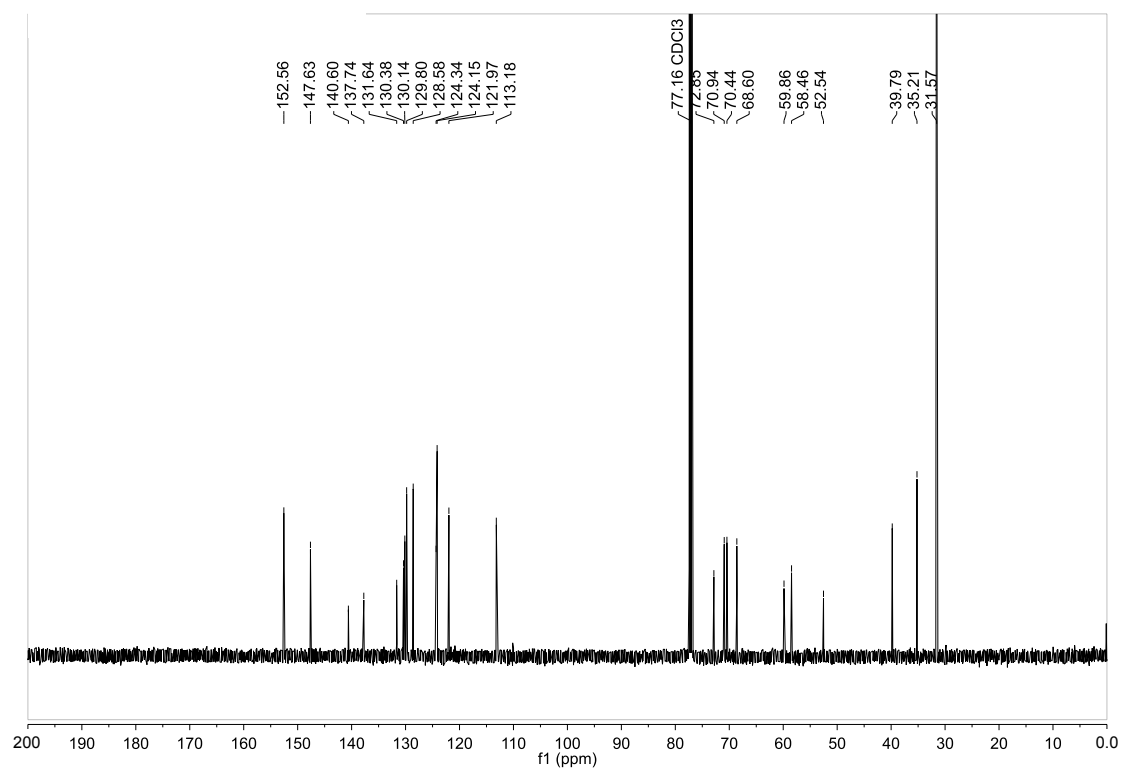


Figure S7. ^{13}C NMR spectrum of $2\text{H}^{3+}\cdot 3\text{I}^-$ (125 MHz, CDCl_3 , 298 K).

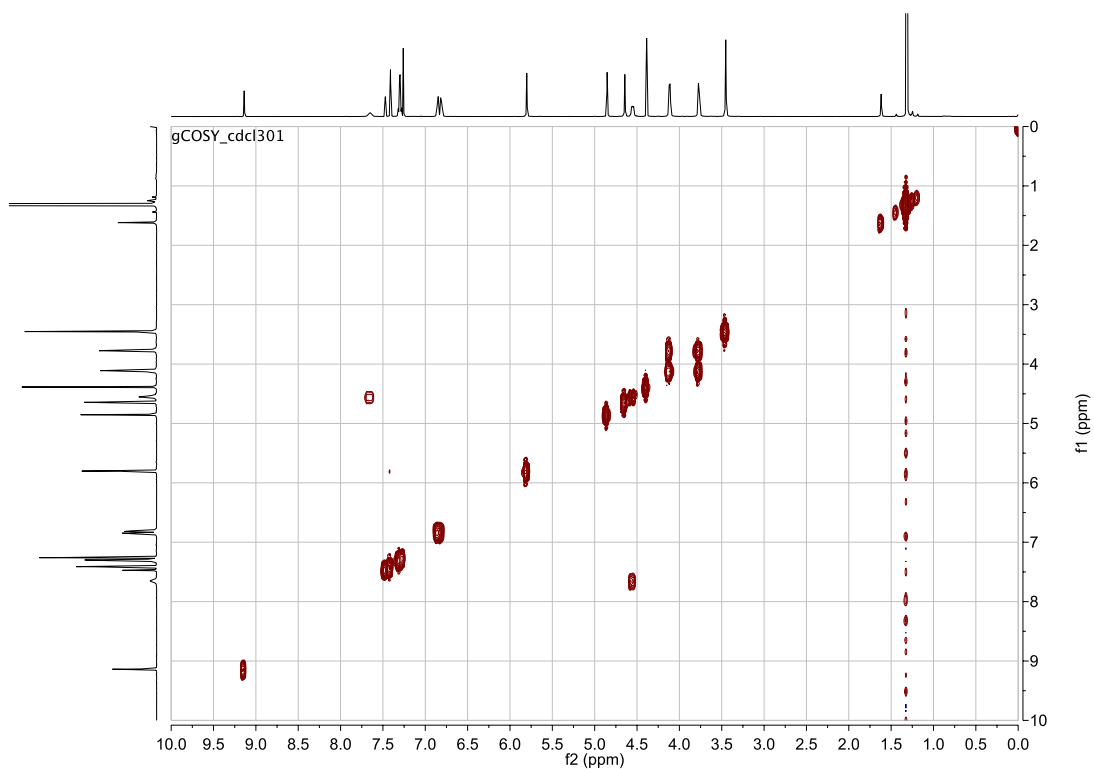


Figure S8. ^1H - ^1H COSY spectrum of $2\text{H}^{3+}\cdot 3\text{I}^-$ (500 MHz, CDCl_3 , 298 K).

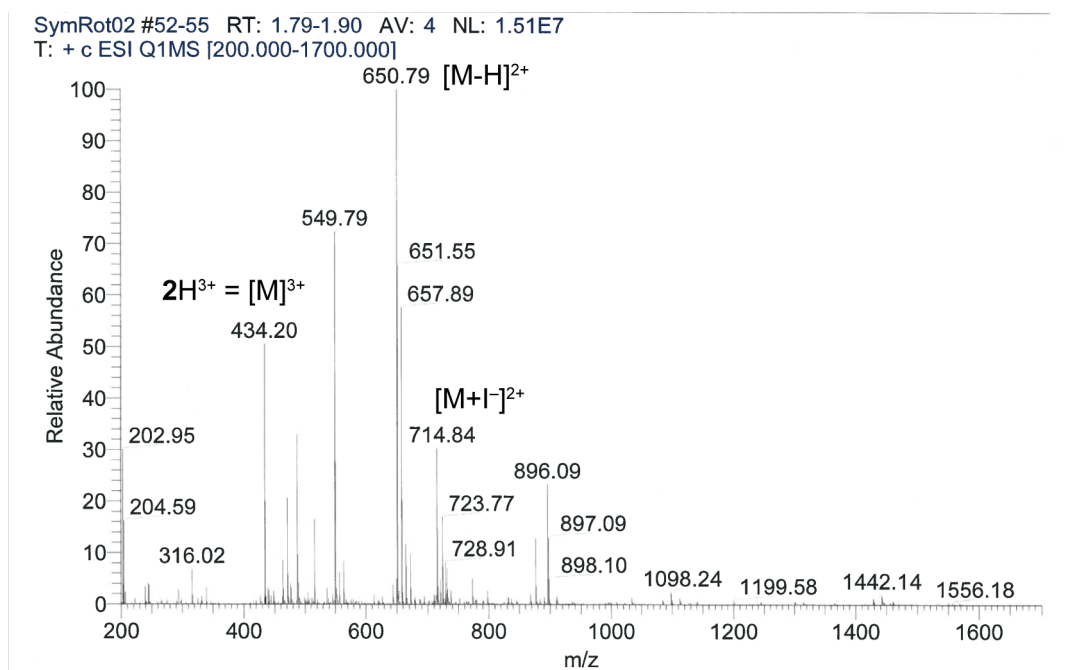


Figure S9. ESI-MS spectrum of $2\text{H}^{3+}\cdot 3\text{I}^-$.

4. Dynamic NMR experiments

4.1. Preparation of 1^{2+} and 2^{2+} by *in situ* deprotonation of $1H^{3+}$ and $2H^{3+}$

$1H^{3+} \cdot 3I^-$ or $2H^{3+} \cdot 3I^-$ (~5 mg) were dissolved in CD_2Cl_2 (0.7 mL) and polymer bound 2-*tert*-butylimino-2-diethylamino-1,3-dimethylperhydro-1,3,2-diazaphosphorine (resin-bound BEMP) was added directly inside the NMR tube. Deprotonation was monitored by 1H -NMR at room temperature following the disappearance of the H_{Tr} (9.08 ppm) proton resonance and the simultaneous appearance of the H_{Tr}^c and H_{Tr}^u (9.29 ppm and 9.16 ppm respectively) resonances (for the protons labelling see main text). The resin was removed by filtration and the resulting solution used in all the subsequent experiments.

4.2. ^1H NMR Characterization of $1^{2+}\cdot 2\text{I}^-$ in CD_2Cl_2 at low temperature

The ^1H NMR, ^1H - ^1H COSY, ^1H - ^1H ROESY, and ^1H - ^1H NOESY spectra of $1^{2+}\cdot 2\text{I}^-$ were acquired at 243 K in CD_2Cl_2 to allow the assignment of proton resonances in the ^1H NMR slow exchange regime.

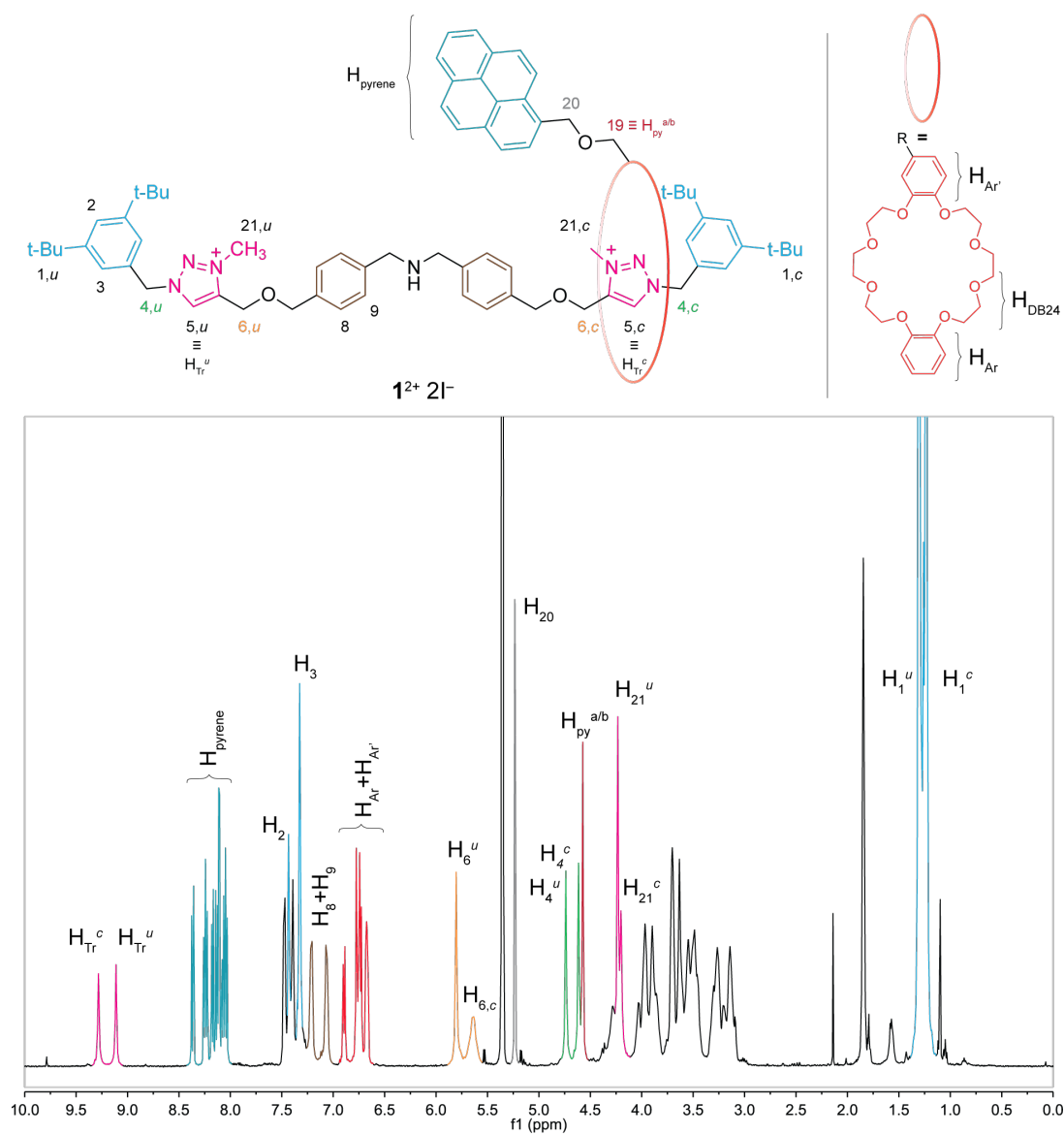


Figure S10. ^1H NMR spectrum of $1^{2+}\cdot 2\text{I}^-$ (500 MHz, CD_2Cl_2 , 243 K). Protons numbering follows the same order as that of $1\text{H}^{3+}\cdot 3\text{I}^-$ (see section 2). Assignment of the signals is color-coded for clarity. Labels c (complexed) and u (uncomplexed).

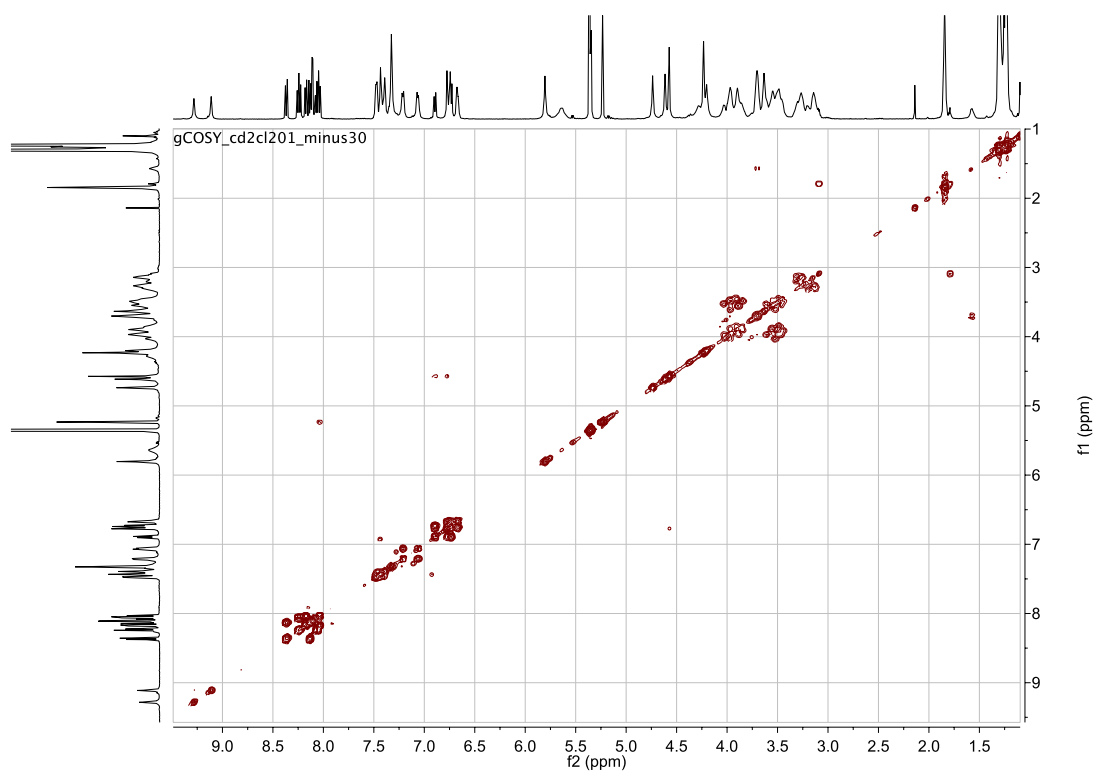


Figure S11. ^1H - ^1H COSY spectrum of $1^{2+} \cdot 2\text{I}^-$ (500 MHz, CD_2Cl_2 , 243 K).

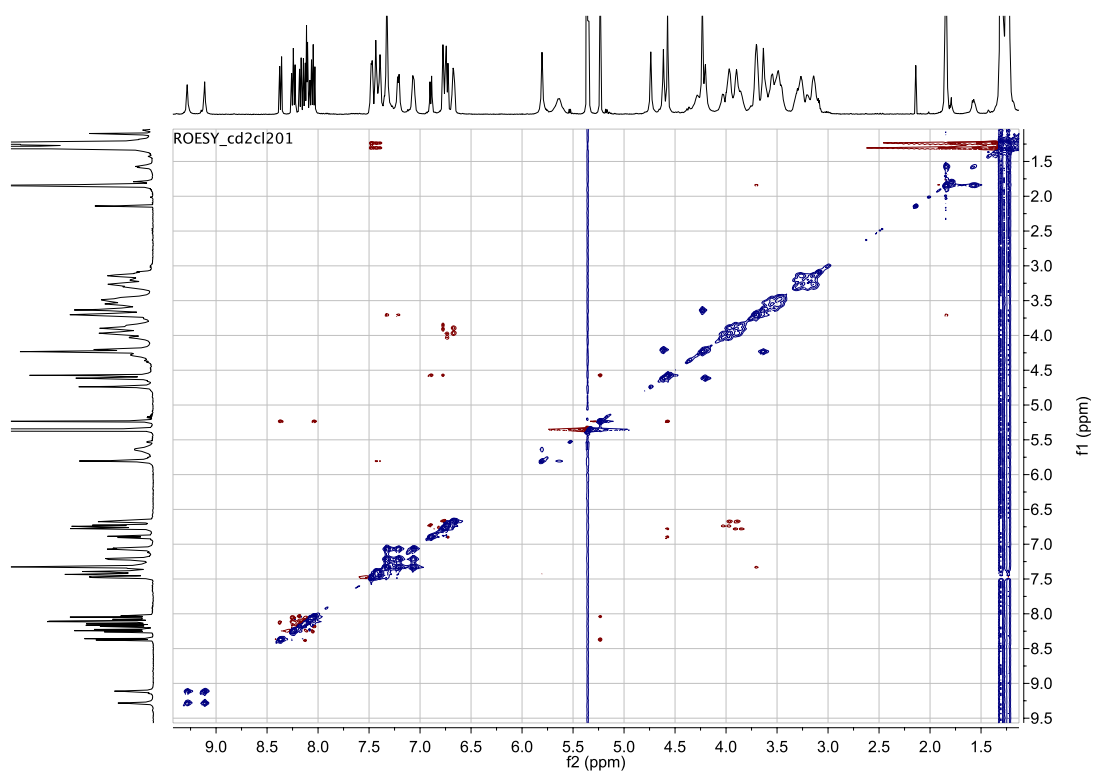


Figure S12. ^1H - ^1H ROESY spectrum of $1^{2+} \cdot 2\text{I}^-$ (500 MHz, CD_2Cl_2 , 243 K, mixing time 400 ms).

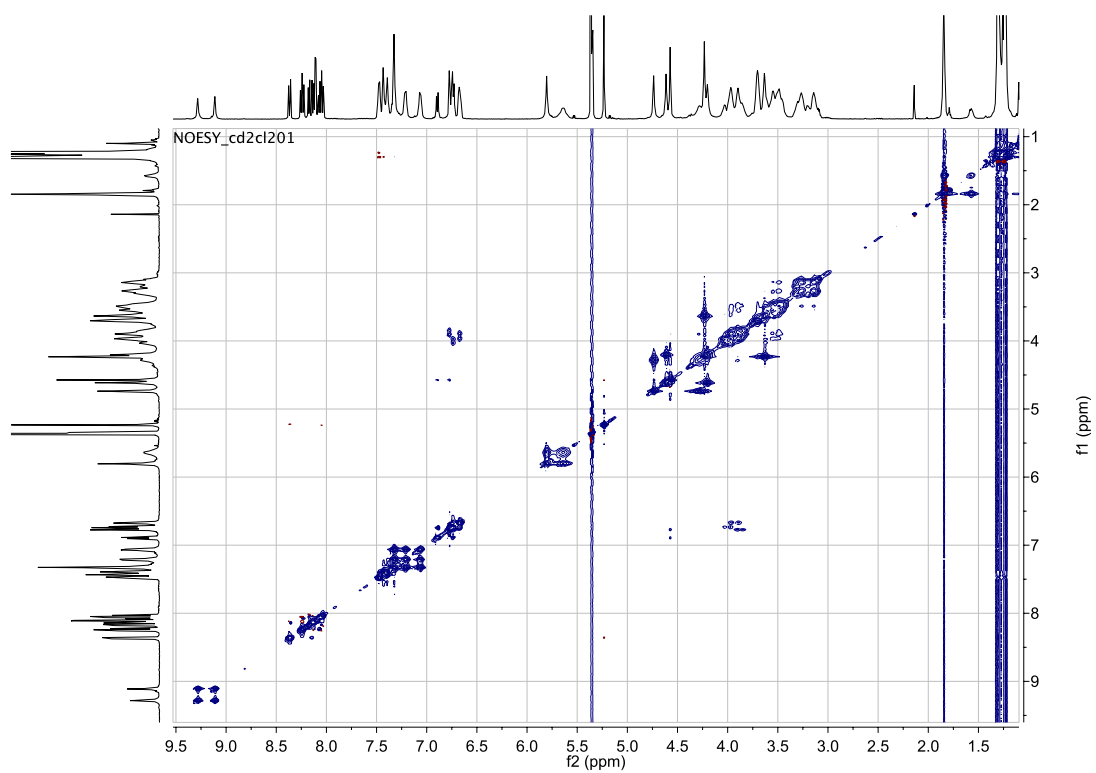


Figure S13. ^1H - ^1H NOESY spectrum of $1^{2+} \cdot 2\text{I}^-$ (500 MHz, CD_2Cl_2 , 243 K, mixing time 400 ms).

4.3. ^1H NMR Characterization of $2^{2+}\cdot 2\text{I}^-$ in CD_2Cl_2 at 213 K

The ^1H NMR spectrum of $2^{2+}\cdot 2\text{I}^-$ was acquired at 213 K in CD_2Cl_2 to allow the assignment of proton resonances in the ^1H NMR slow exchange regime.

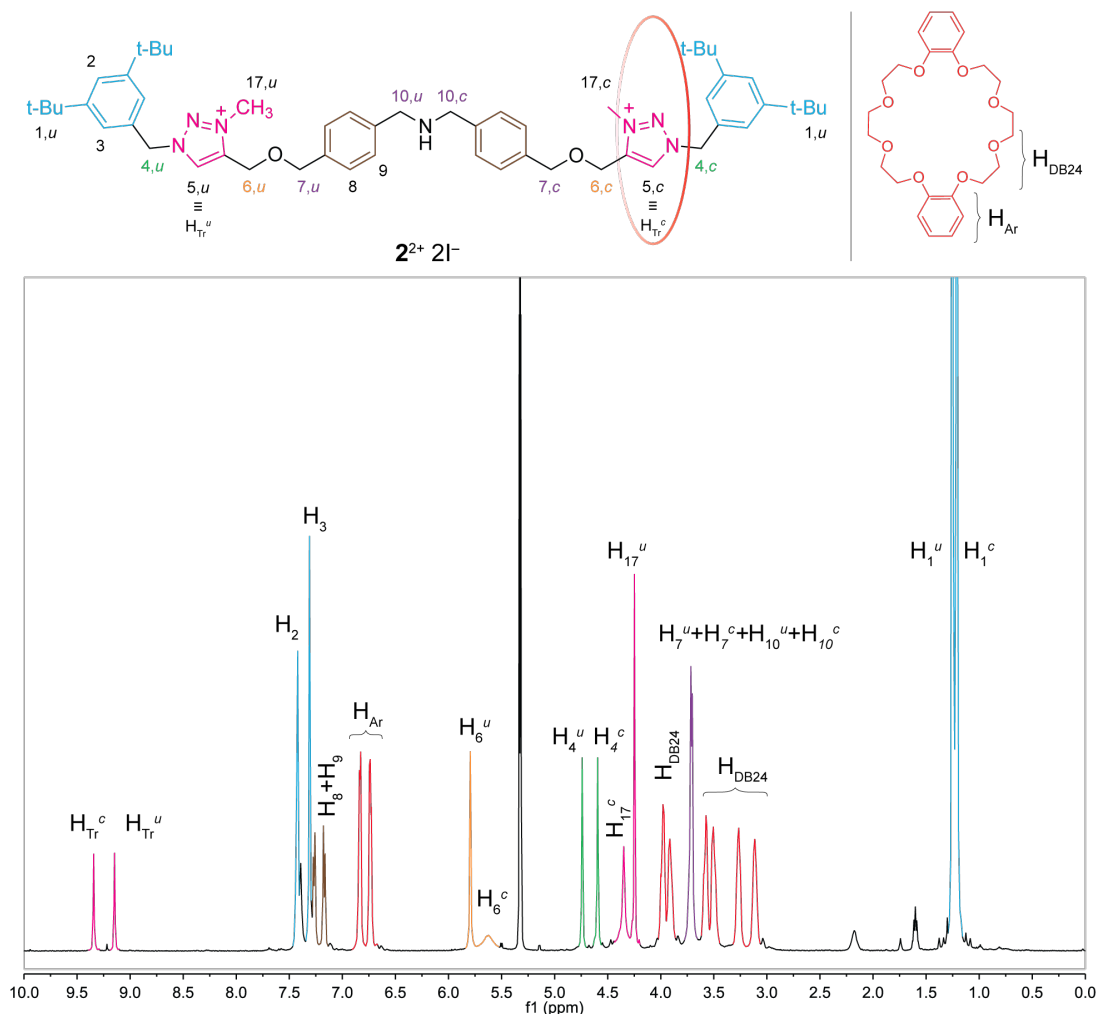


Figure S14. ^1H NMR spectrum of $2^{2+}\cdot 2\text{I}^-$ (500 MHz, CD_2Cl_2 , 213 K). Proton numbering follows the same order as that of 2H^{3+} (see section 2). Assignment of the signals is color-coded for clarity. Labels c (complexed) and u (uncomplexed).

4.4. Reversible pH dependent co-conformational switching

A fresh sample of $1\text{H}^{3+}\cdot 3\text{I}^-$ dissolved in CD_2Cl_2 was deprotonated with BEMP resin. The ^1H NMR spectra was recorded at 213 K and then a small amount of $\text{CF}_3\text{CO}_2\text{D}$ was added to protonate the free secondary amine and regenerate 1H^{3+} . Minor variations in the resonance frequency of signals in spectra reported in Figure S15a and S15c are due to the presence of trifluoroacetate counteranions.

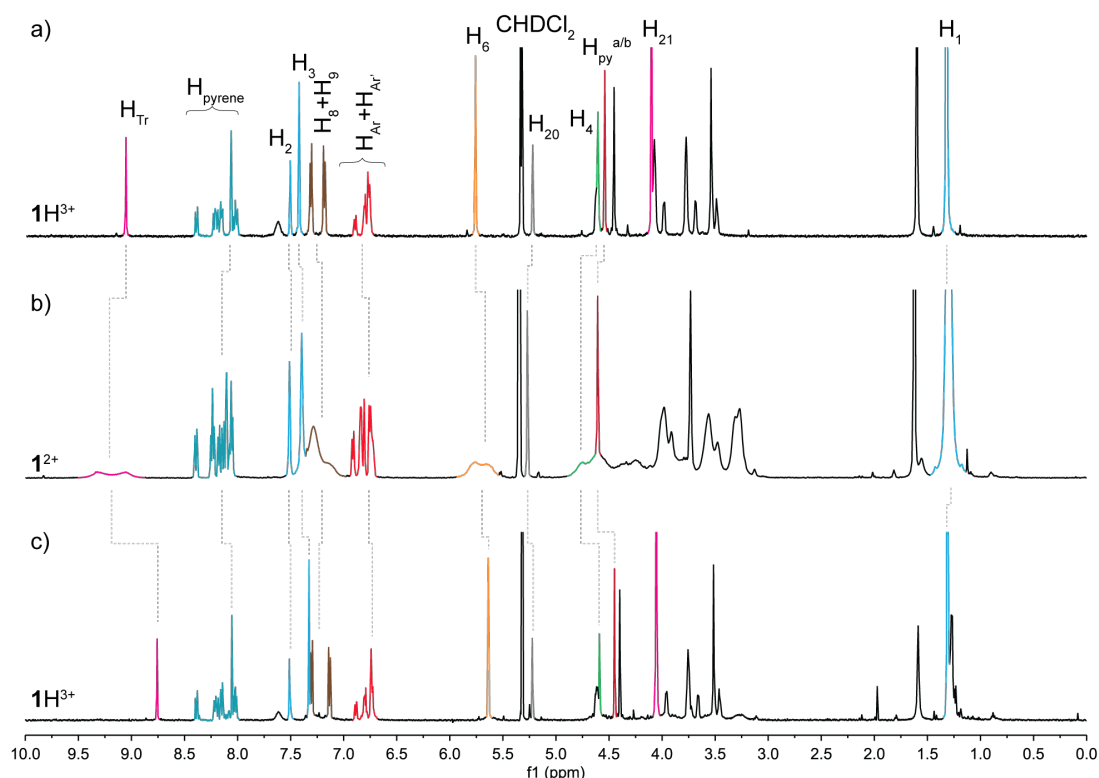


Figure S15. ^1H NMR (500 MHz, CD_2Cl_2 , 298 K) spectra of a) $1\text{H}^{3+}\cdot 3\text{I}^-$, b) the same sample after deprotonation with resin-bound BEMP and c) after protonation with $\text{CF}_3\text{CO}_2\text{D}$. Proton resonances are labelled according to Figure S8.

4.5. Variable temperature NMR spectra

^1H NMR spectra of $1^{2+}\cdot 2\text{I}^-$ and $2^{2+}\cdot 2\text{I}^-$ in CD_2Cl_2 were recorded between 223 K and 293 K at 10 K intervals to elucidate the dynamics of the systems. Co-conformational switching rates were calculated from a line-shape analysis of the variable temperature NMR spectra using TOPSPIN 3.5 software. The enthalpy (ΔH^\ddagger) and entropy (ΔS^\ddagger) of activation for ring shuttling were extrapolated by fitting the Eyring plots of shuttling rate vs the reciprocal of absolute temperature using the following equation (R is the ideal gas constant, h is Plank's constant, and k_B is Boltzmann's constant).

$$\ln\left(\frac{k_{sh}}{T}\right) = -\frac{\Delta H^\ddagger}{RT} + \frac{\Delta S^\ddagger}{R} + \ln\frac{k_B}{h}$$

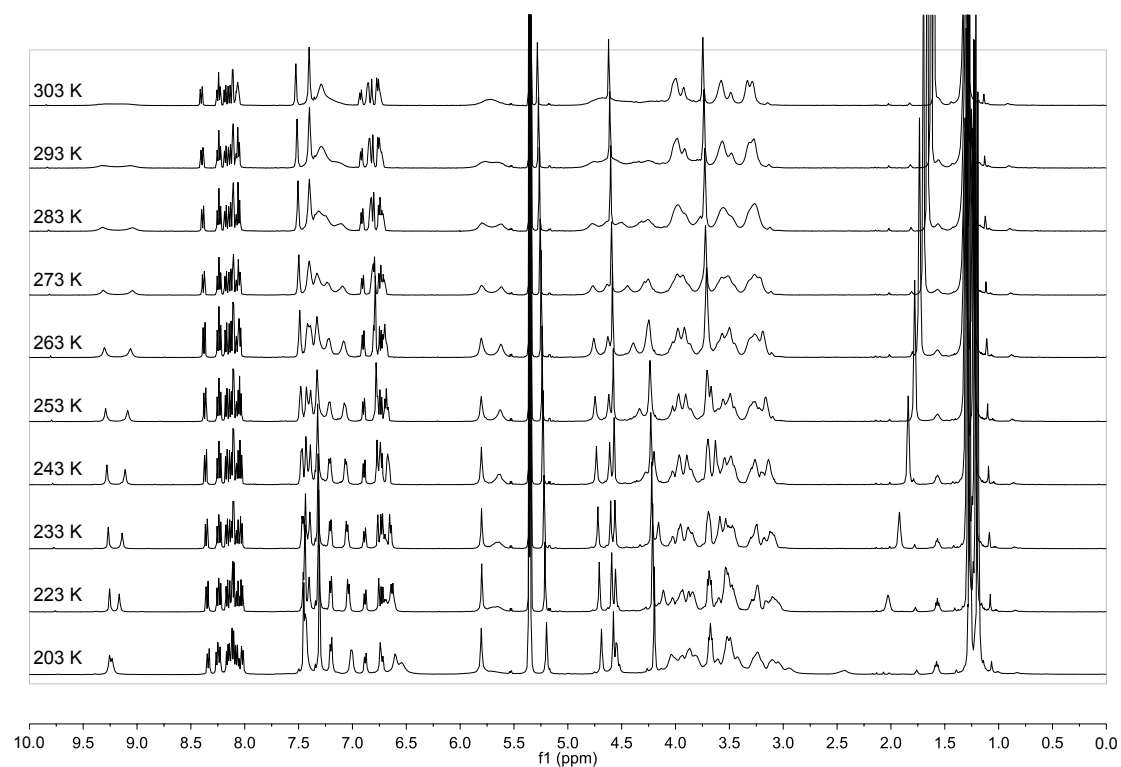


Figure S16. Variable temperature $^1\text{H-NMR}$ spectra of $1^{2+} \cdot 2\Gamma$ (500 MHz, CD_2Cl_2).

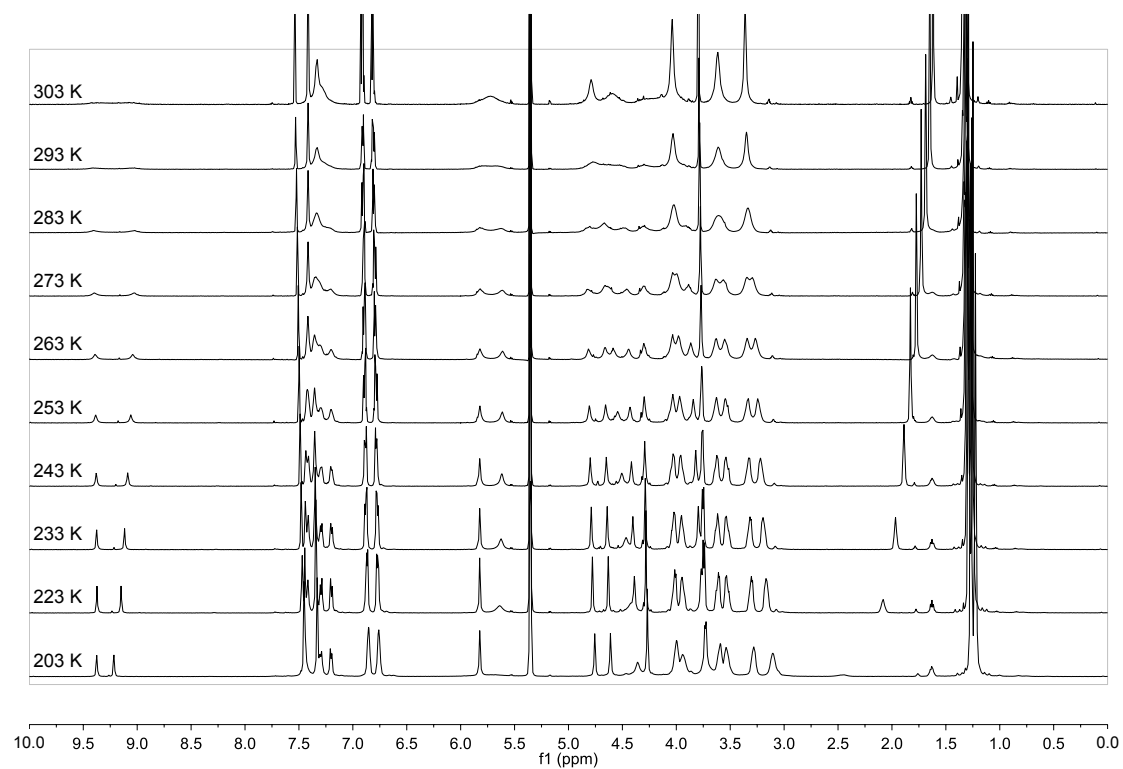


Figure S17. Variable temperature $^1\text{H-NMR}$ spectra of $2^{2+} \cdot 2\Gamma$ (500 MHz, CD_2Cl_2).

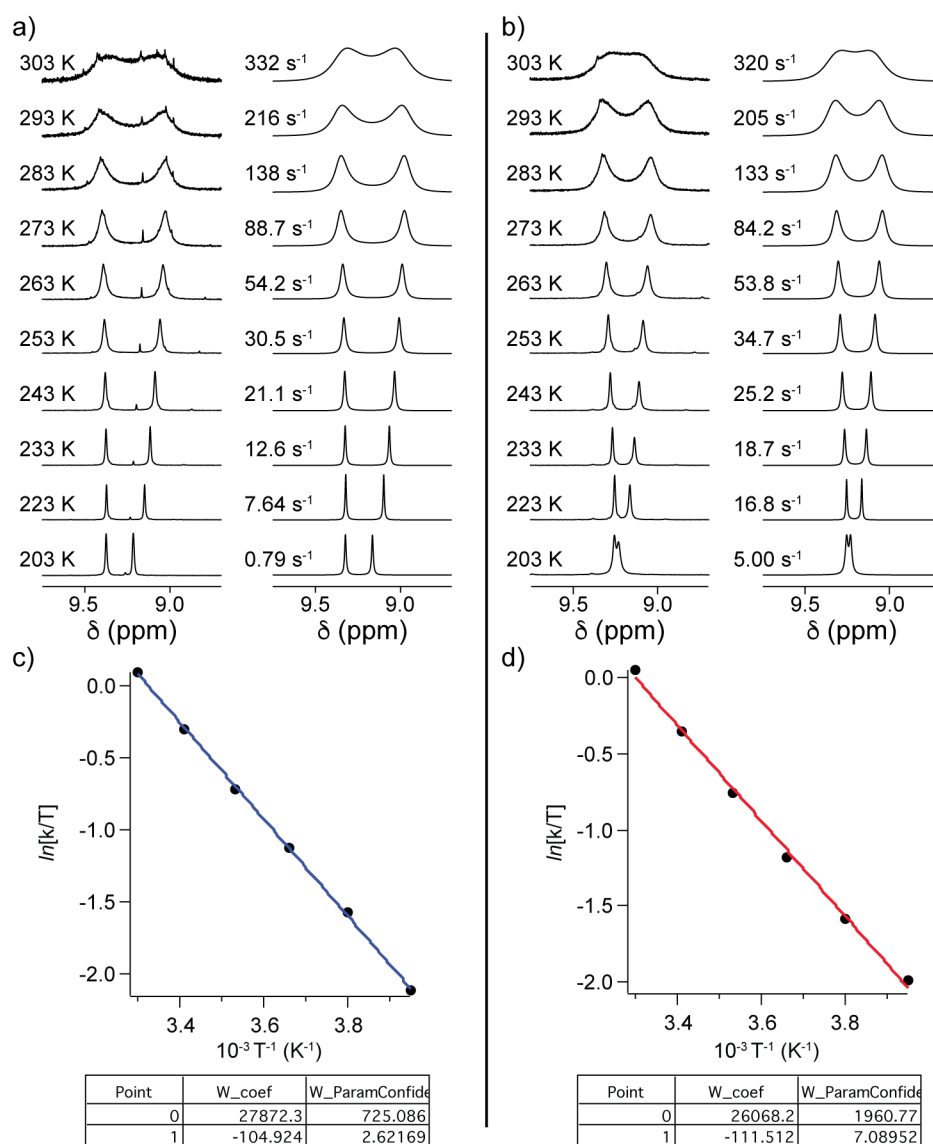


Figure S18. Partial $^1\text{H-NMR}$ (500 MHz, CD_2Cl_2) spectra of a) $2^{2+}\cdot 2\text{I}^-$ and b) $1^{2+}\cdot 2\text{I}^-$ at different temperatures (left) and corresponding simulated NMR spectra of the exchanging protons H_{Tr}^u and H_{Tr}^c (right). Exchange rate constants (k_{sh}) are reported (right column, for assignment see text). c) Eyring plot of the shuttling process in $2^{2+}\cdot 2\text{I}^-$. $\Delta H^\ddagger = 27.9 \text{ kJ mol}^{-1}$, $\Delta S^\ddagger = -105 \text{ J mol}^{-1} \text{ K}^{-1}$. d) Eyring plot of the shuttling process in $1^{2+}\cdot 2\text{I}^-$. $\Delta H^\ddagger = 26.1 \text{ kJ mol}^{-1}$, $\Delta S^\ddagger = -112 \text{ J mol}^{-1} \text{ K}^{-1}$.

The H_{Tr}^u signal is the weighted average of the signal of the unencircled triazolium protons in the tightly bound and solvent separated ion pairs in fast chemical exchange.⁶ Its downfield shift at temperatures lower than 253 K arises from the displacement of the equilibrium between the tight and separated ion pairs in favor of the former. Therefore, the Eyring analysis was performed only taking into account the data at temperatures ranging from 303 K to 253 K, where the drift of the signals can be neglected. In this range, the shape of the signals is dominated by the co-conformational equilibrium and line-shape analysis provides reliable results (Figure S18). Noteworthy, the resonance frequency of H_{Tr}^c is unaffected by temperature, suggesting that anions cannot reach the first coordination sphere of the complexed triazolium station because of the presence of the surrounding ring.

4.6 Estimation of the racemization rate constant

The rate constant of racemization k_{rac} of about 35 s^{-1} was estimated at the coalescence temperature (ca. 243 K) using the following formula:

$$k_{\text{rac}} = 2.22 \sqrt{\Delta\nu^2 + (J_{\text{AB}})^2} = 35 \text{ s}^{-1}$$

The resonances of H_4^{c} , $\text{H}_{\text{Py}}^{\text{a}}$, and $\text{H}_{\text{Py}}^{\text{b}}$ are partially overlapped, therefore for a more accurate estimation of the $\text{H}_{\text{Py}}^{\text{a}} - \text{H}_{\text{Py}}^{\text{b}}$ $\Delta\nu \approx 12 \text{ Hz}$ and $J_{\text{AB}} \approx 10 \text{ Hz}$ in the slow exchange regime, the spin system was simulated (Figure S19).

The line-shape analysis of the $\text{H}_{\text{Tr}}^{\text{u/c}}$ resonances (Figure 2b in the main text) revealed that, at the coalescence temperature of the $\text{H}_{\text{Py}}^{\text{a/b}}$ resonances (243 K), the rate constant for ring shuttling is around 25 s^{-1} , which is comparable with the racemization rate constant calculated above.

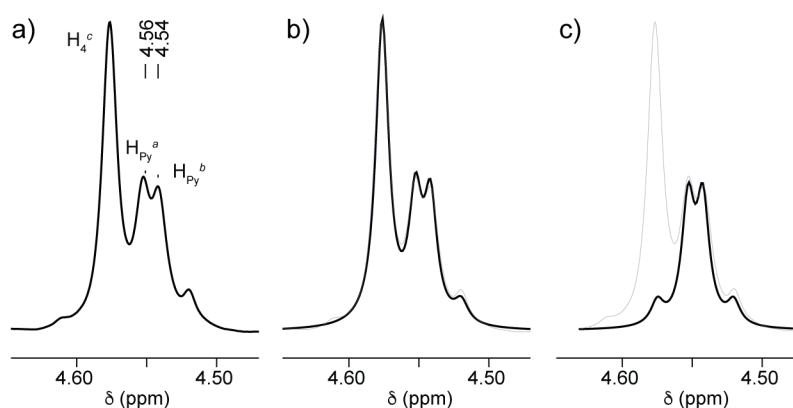


Figure S19. a) Partial ¹H-NMR (500 MHz, CD₂Cl₂, 203 K) spectra of $\mathbf{1}^{2+} \cdot 2\text{I}^-$. b) Simulated spectra of the overlapping H_4^{c} proton resonance with the AB spin system of the diastereotopic protons $\text{H}_{\text{Py}}^{\text{a}}$ and $\text{H}_{\text{Py}}^{\text{b}}$. c) Deconvolution of the aforementioned resonances.

Despite the NMR resolution was not high enough to resolve the fine structure, the resonance H_6^{c} of $\mathbf{1}^{2+} \cdot 2\text{I}^-$ consistently appears to be structured as two doublets of an AB system at 233 K (figure S20a). Conversely, the corresponding signal in the symmetric rotaxane $\mathbf{2}^{2+} \cdot 2\text{I}^-$ always appears as a broad singlet (Figure S20b). This is consistent with the two protons H_6^{c} being diastereotopic in $\mathbf{1}^{2+} \cdot 2\text{I}^-$ and enantiotopic, thus identical, in $\mathbf{2}^{2+} \cdot 2\text{I}^-$.

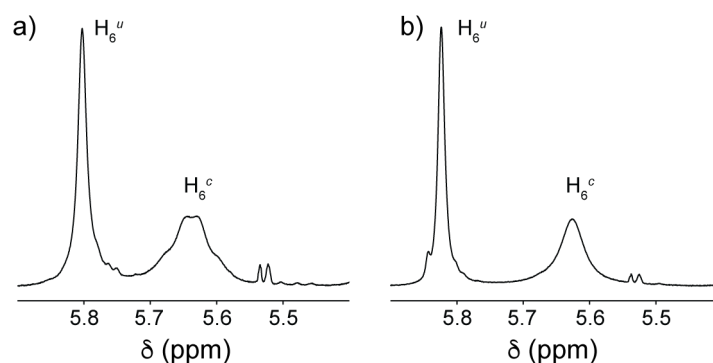


Figure S20. Partial ¹H-NMR (500 MHz, CD₂Cl₂, 233 K) spectra of a) $\mathbf{1}^{2+} \cdot 2\text{I}^-$ and b) $\mathbf{2}^{2+} \cdot 2\text{I}^-$ highlighting the region of H_6 protons.

4.7 ^1H NMR spectra of $1^{2+}\cdot 2\text{I}^-$ and $2^{2+}\cdot 2\text{I}^-$ in the presence of (+)-CS and (-)-CS in CD_2Cl_2

The ^1H NMR spectra of $1^{2+}\cdot 2\text{I}^-$ and $2^{2+}\cdot 2\text{I}^-$ were recorded at 243 K and 223 K prior and after addition of 8 equivalents of tetrabutylammonium (+)-camphorsulfonate [(+)-CS] or (-)-camphorsulfonate [(-)-CS]. For the sake of clarity, in the following figures samples were named $1^{2+}\cdot 2[(+)\text{-CS}]$, $1^{2+}\cdot 2[(-)\text{-CS}]$, and $2^{2+}\cdot 2[(+)\text{-CS}]$ respectively. Deprotonation was performed according to the protocol reported in section 4.1.

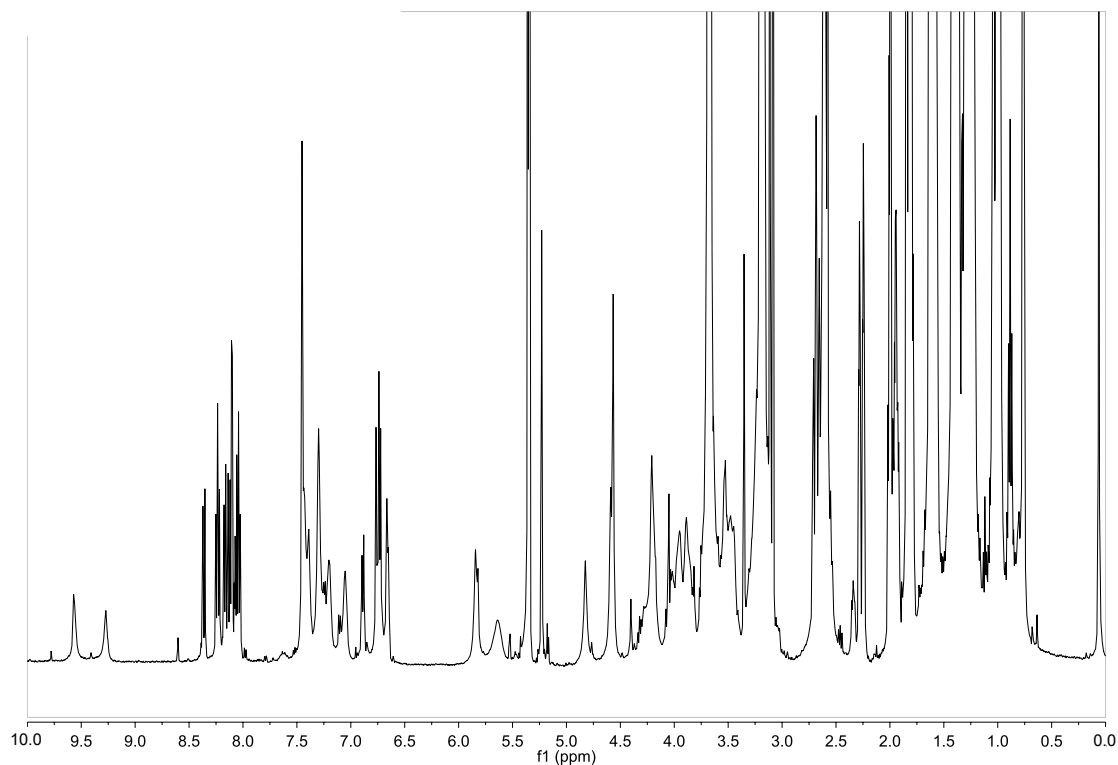


Figure S21. ^1H NMR spectrum of $1^{2+}\cdot 2[(+)\text{-CS}]$ (500 MHz, CD_2Cl_2 , 243 K).

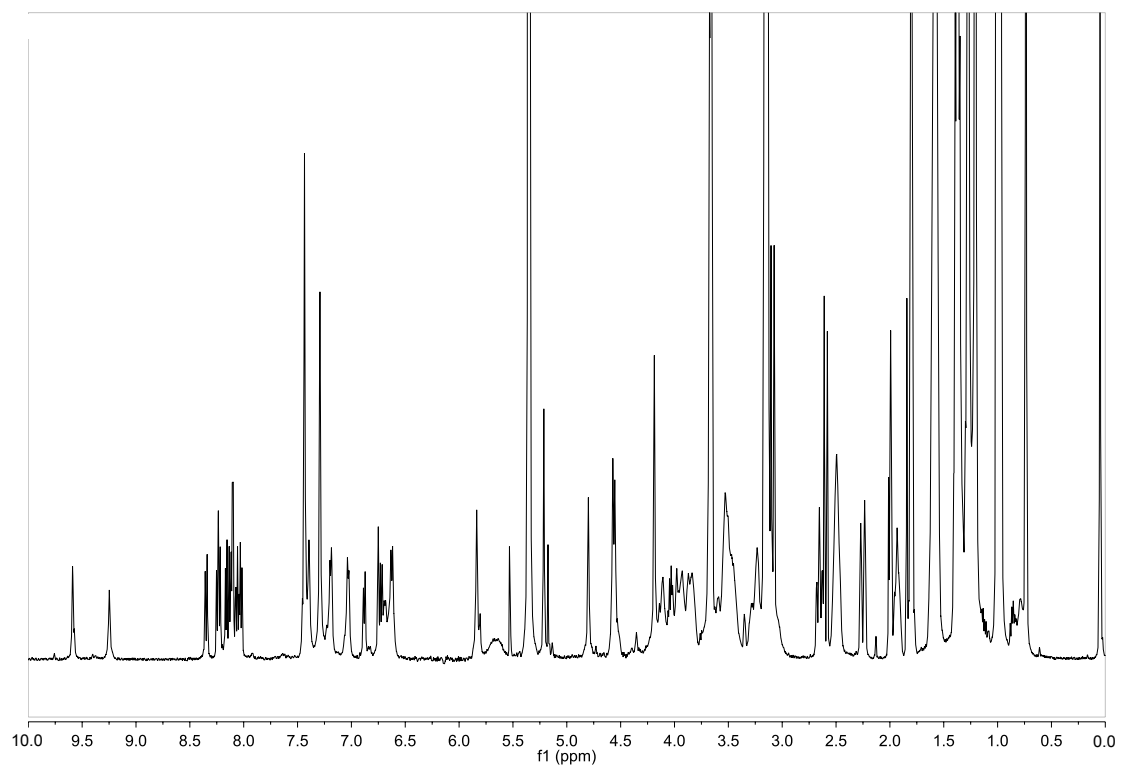


Figure S22. ^1H NMR spectrum of $1^{2+}\cdot 2[(+)\text{-CS}]$ (500 MHz, CD_2Cl_2 , 223 K).

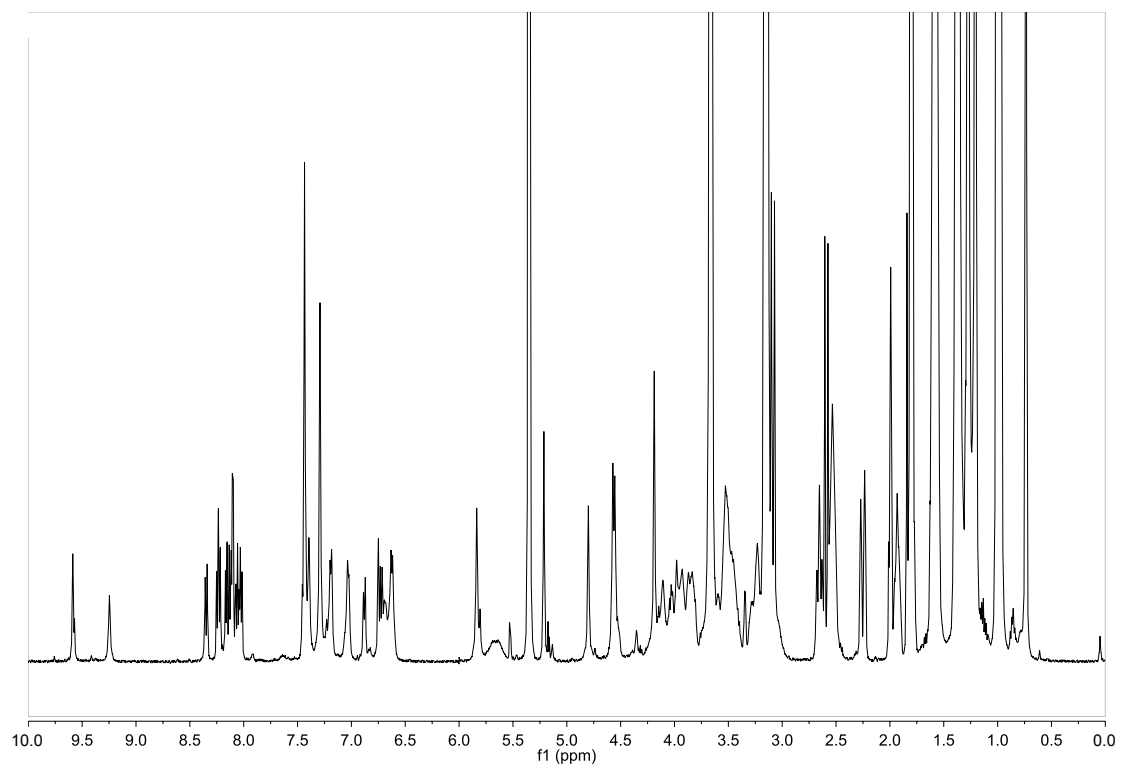


Figure S23. ^1H NMR spectrum of $1^{2+}\cdot 2[(-)\text{-CS}]$ (500 MHz, CD_2Cl_2 , 223 K).

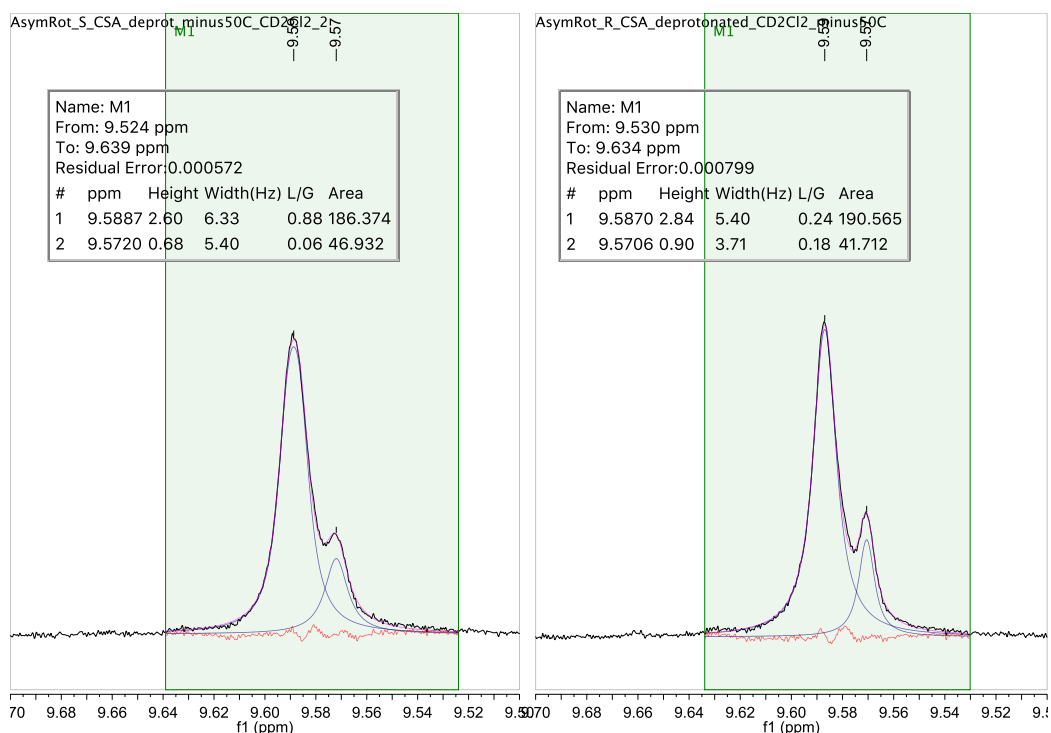


Figure S24. Partial ¹H NMR spectrum of the proton resonance H_{Tr}^u in 1²⁺·2[(+)-CS] (left) and 1²⁺·2[(-)-CS] (right) and deconvolution for the determination of the diastereomeric ratio (500 MHz, CD₂Cl₂, 223 K).

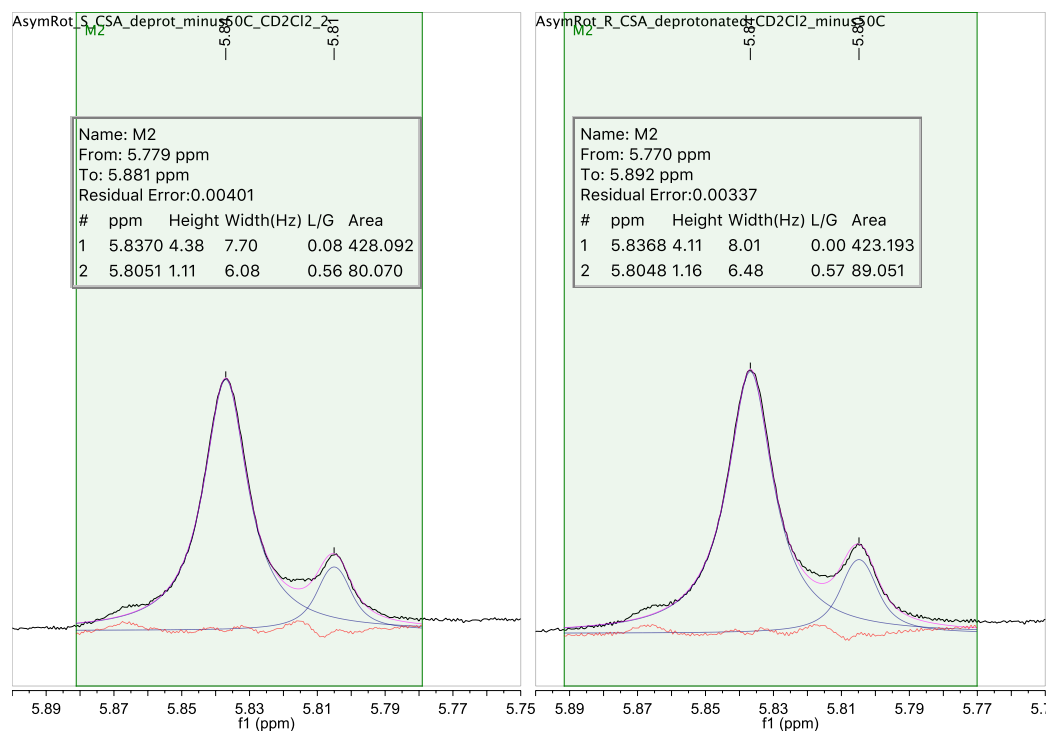
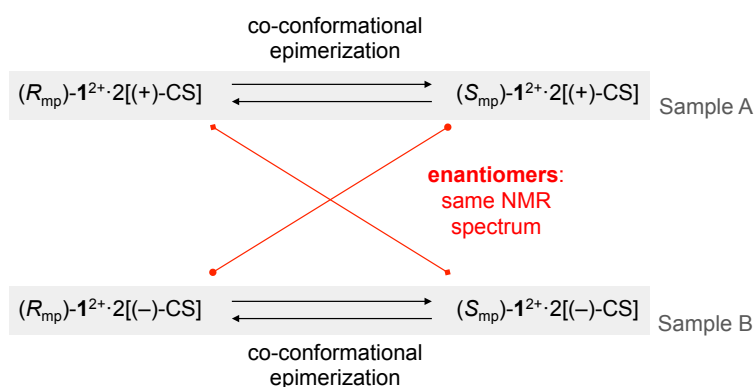


Figure S25. Partial ¹H NMR spectrum of the proton resonance H₆^u in 1²⁺·2[(+)-CS] (left) and 1²⁺·2[(-)-CS] (right) and deconvolution for the determination of the diastereomeric ratio (500 MHz, CD₂Cl₂, 223 K).

The d.r. at 223 K, determined from measurements performed on six different NMR samples prepared independently by using two different synthetic batches, was found to be 85:15, with a standard deviation of 4% on the percentage of the individual diastereomers. The corresponding

value of $\Delta\Delta G^\circ$ at 223 K is 3.2 kJ mol⁻¹ with a standard deviation of 0.7 kJ mol⁻¹.

The spectra recorded for $1^{2+}\cdot 2[(+)\text{-CS}]$ and $1^{2+}\cdot 2[(-)\text{-CS}]$ are identical within error both in terms of chemical shift and integral ratio. This result is fully consistent with the formation of two pairs of diastereomeric salts that exhibit enantiomeric relations with one another, as expected in the present case (Scheme S3). In fact $(R_{\text{mp}})\text{-}1^{2+}\cdot 2[(+)\text{-CS}]$ and $(S_{\text{mp}})\text{-}1^{2+}\cdot 2[(+)\text{-CS}]$, as well as $(R_{\text{mp}})\text{-}1^{2+}\cdot 2[(-)\text{-CS}]$ and $(S_{\text{mp}})\text{-}1^{2+}\cdot 2[(+)\text{-CS}]$, are enantiomeric pairs and thus display the same NMR spectrum (Scheme S3). In addition the diastereomers of each pair, that epimerize *via* ring shuttling, must have the same relative stabilities and therefore are formed in the same ratio, regardless of the absolute configuration of the added camphorsulfonate salt.



Scheme S3. Possible diastereomeric salts formed by the mechanically planar chiral rotaxane 1^{2+} in the presence of the optically active camphorsulfonate anion. Samples A and B refer to the addition of 8 equivalents of tetrabutylammonium (+)-CS and (-)-CS, respectively, to $1^{2+}\cdot 2\text{I}^-$.

In order to exclude that the appearance of a new set of resonances – in particular for H_{Tr}^u and H_6^u – is due to a (admittedly unlikely) slow exchange in the NMR timescale between the bound and unbound ion pairs, or between different ion pairs, [(+)-CS] was added to rotaxane $2^{2+}\cdot 2\text{I}^-$, which does not possess chiral co-conformations and cannot form diastereomeric salts. Only a downfield shift of the H_{Tr}^u resonance was observed, confirming the rather strong interaction of the free triazolium station with the sulfonate anion. However, no new resonances were observed for protons H_{Tr}^u or H_6^u at any temperature (Figure S26).

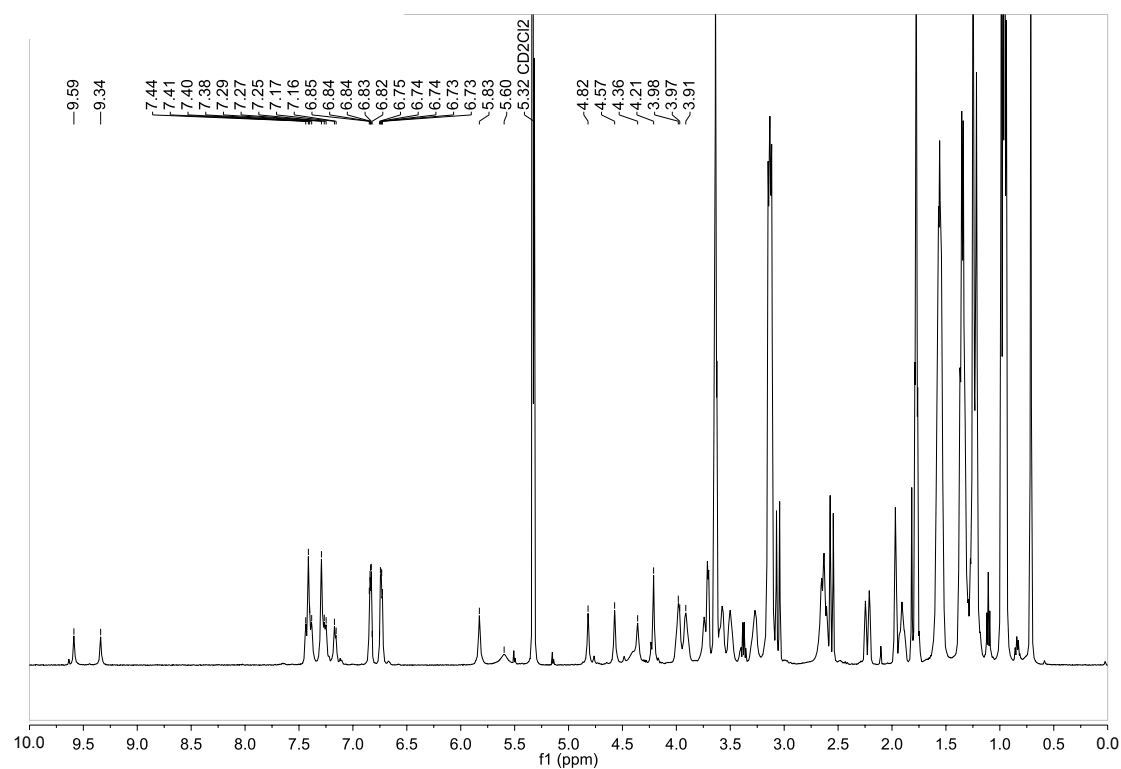


Figure S26. ^1H NMR spectrum of $2^{2+}\cdot 2[(+)\text{-CS}]$ (500 MHz, CD_2Cl_2 , 223 K).

Additionally, a sample of $1^{2+}\cdot 2[(-)\text{-CS}]$ was protonated by adding ~ 1 equivalent of $(-)$ -camphorsulfonic acid. Upon protonation only one set of resonances for both H_{Tr} and H_6 was detected. Such an observation proves that the anions are in fast exchange with the triazolium in the NMR timescale. The slight downfield shift from 9.14 ppm ($1\text{H}^{3+}\cdot 3\text{I}^-$) to 9.18 ppm is perfectly in line with the change in anion concentration. Incidentally this result also confirms the reversibility of the chiral recognition process (Figure S26).

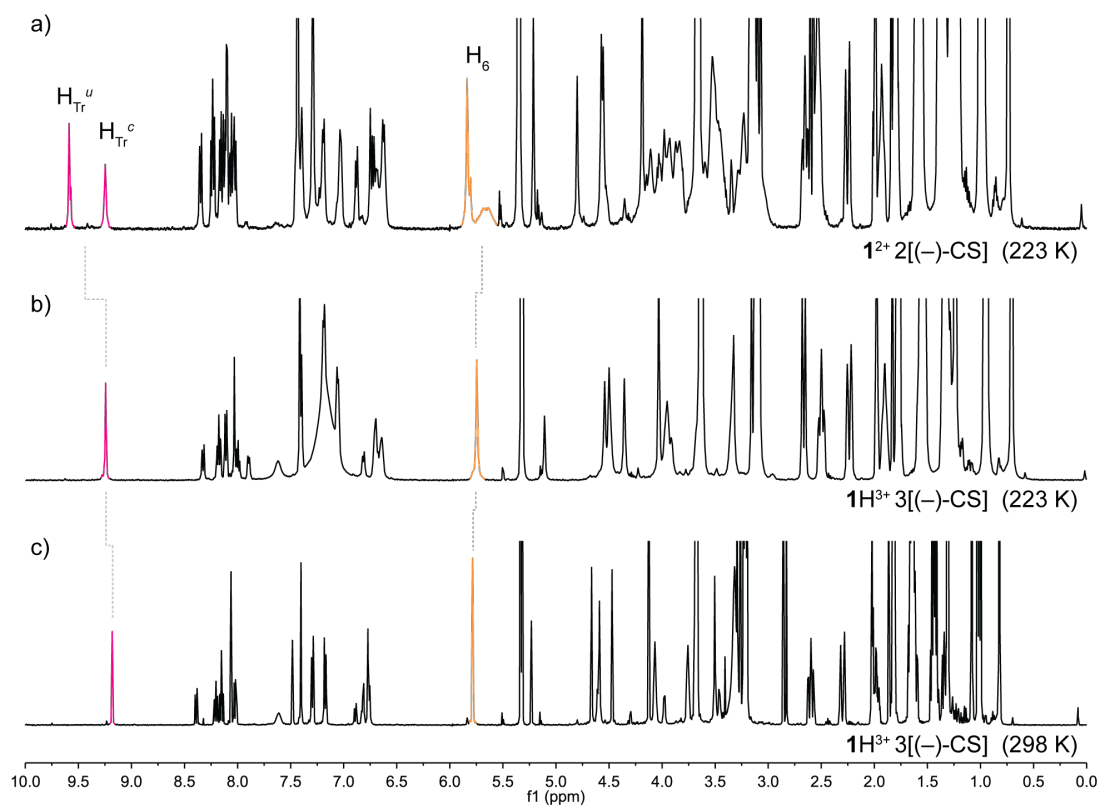


Figure S27. a) ^1H NMR spectrum of $1^{2+}\cdot 2[(-)\text{-CS}]$ (500 MHz, CD_2Cl_2 , 223 K). Parts b) and c) show the spectra of the same sample after protonation with $(-)$ -camphorsulfonic acid at 223 K and 298 K, respectively (500 MHz, CD_2Cl_2).

In order to study the dynamics of the interconversion between the diastereomeric forms of $1^{2+} \cdot 2[(-)\text{-CS}]$, ^1H NMR spectra were recorded at temperatures between 233 K and 278 K at 5 K intervals (Figure S28 and S29).

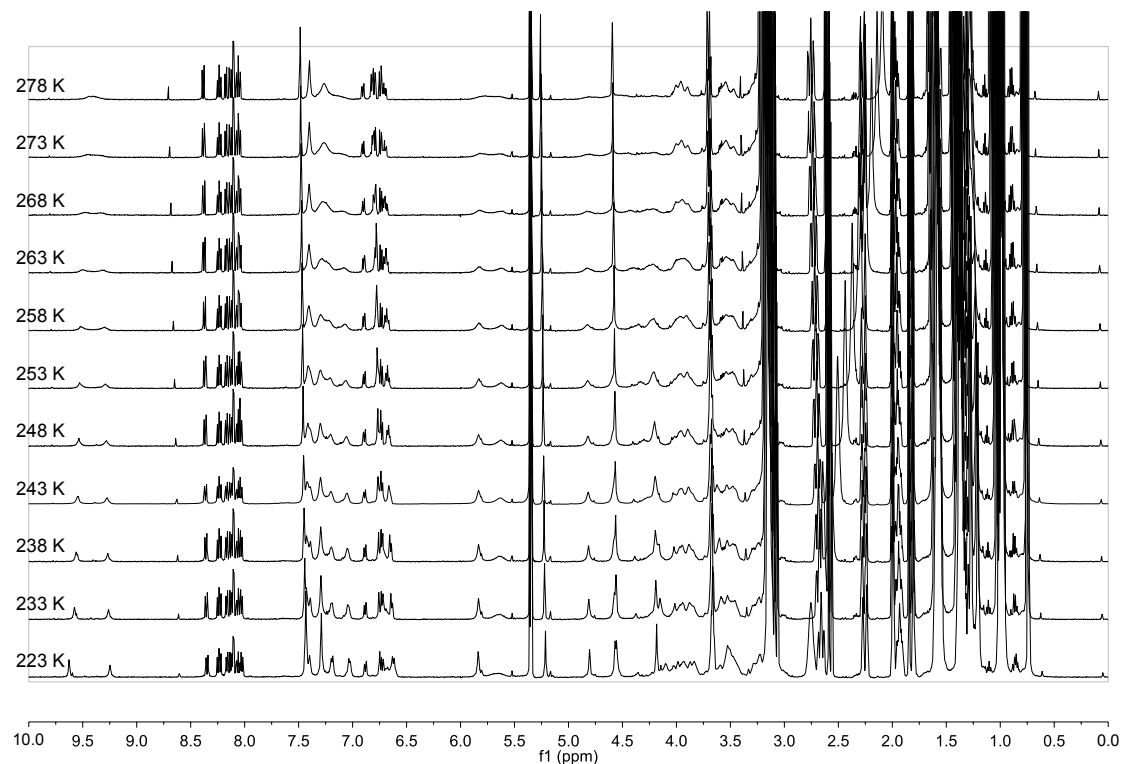


Figure S28. Variable temperature ^1H -NMR spectra of $1^{2+} \cdot 2[(-)\text{-CS}]$ (500 MHz, CD_2Cl_2). The ^1H -NMR spectrum at 223 K was also recorded for consistency.

When the shuttling process becomes fast in the NMR timescale, the NMR spectrum in fast exchange reflects an average structure where the ring is located in the middle of the axle. In other words the residual symmetry of the system renders the rotaxane achiral on average. Therefore, the diastereomeric ion pairs formed by interaction with an optically active anion are not detectable anymore as they are interconverting into one another too fast. As a consequence, the four signals $H_{\text{Tr,major}}^u$, $H_{\text{Tr,major}}^c$, $H_{\text{Tr,minor}}^u$, $H_{\text{Tr,minor}}^c$, display the same coalescence temperature (273 K), as can be seen in Figure S29a. It is noteworthy that resonances $H_{\text{Tr,major}}^u$ and $H_{\text{Tr,minor}}^u$ coalesce with their respective complexed stations ($H_{\text{Tr,major}}^c$, $H_{\text{Tr,minor}}^c$) and not with each other. The corresponding H_6 signals also display a single coalescence temperature (278 K). Furthermore, the d.r. evaluated in the slow exchange NMR regime does not vary within the experimental error (Figures S29b and S30b), indicating that $\Delta\Delta G^\circ$ is almost constant over the 223-243 K range.

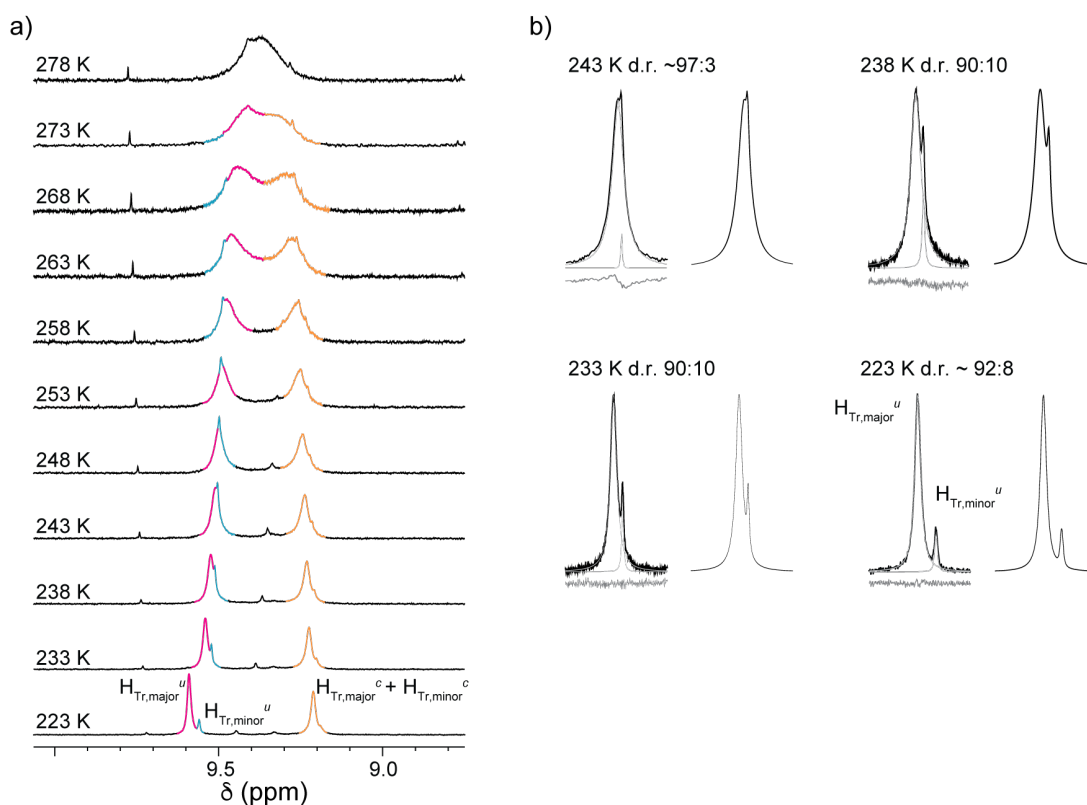


Figure S29. a) Partial ¹H-NMR spectra of $1^{2+} \cdot 2[(-)-CS]$ (500 MHz, CD_2Cl_2) at different temperatures in the region of $H_{Tr,major}^u$, $H_{Tr,major}^c$, $H_{Tr,minor}^u$, and $H_{Tr,minor}^c$. b) Deconvolution (left column) and fit result (right column) of $H_{Tr,major}^u$ and $H_{Tr,minor}^u$ resonances for the determination of the d.r. at 223, 233, 238 and 243 K.

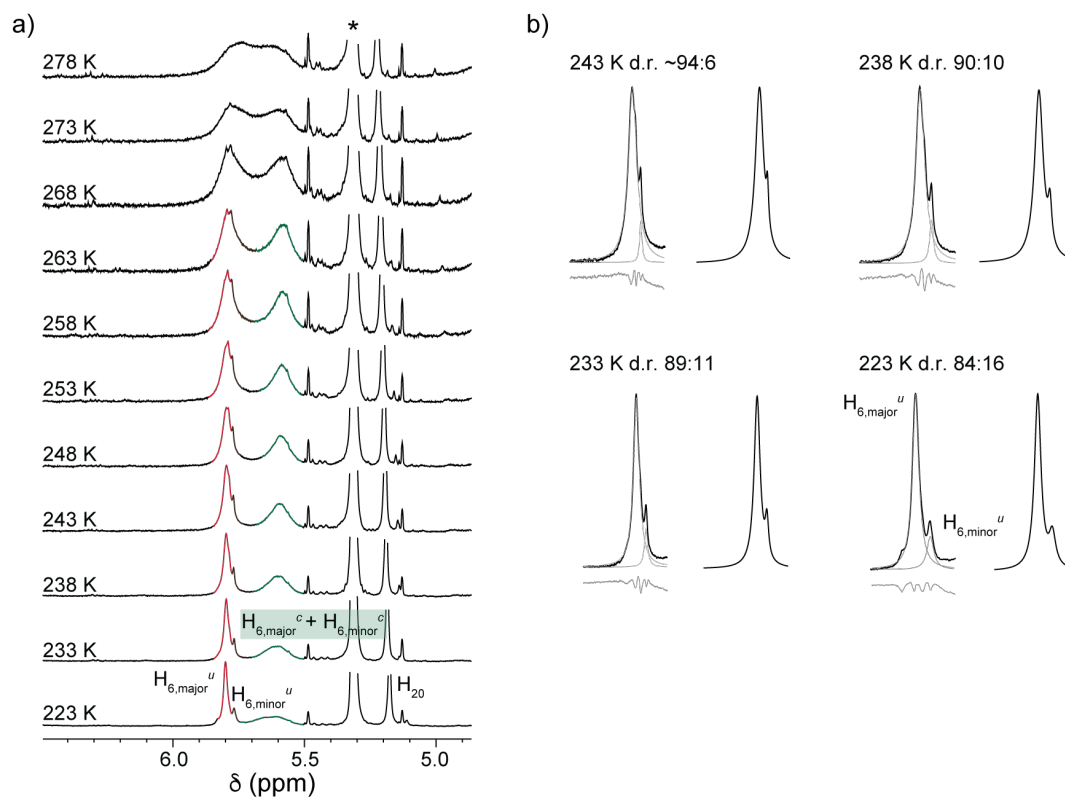
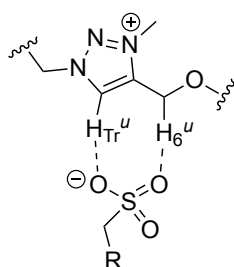


Figure S30. a) Partial ¹H-NMR spectra of $1^{2+} \cdot 2[(-)-CS]$ (500 MHz, CD_2Cl_2) at different temperatures in the region of $H_{6,major}^u$, $H_{6,major}^c$, $H_{6,minor}^u$, and $H_{6,minor}^c$. b) Deconvolution (left column) and fit result (right column) of $H_{6,major}^u$ and $H_{6,minor}^u$ resonances for the determination of the d.r. at 223, 233, 238 and 243 K. The signal marked with an asterisk is the residual solvent peak.

The spectra recorded with intermediate concentrations of tetrabutylammonium (TBA) (–)-camphorsulfonate showed a downfield shift of the resonance associated with H_{Tr}^u with increasing amount of [(–)-CS] (Figures S31 and S32). This is consistent with the ion pairing equilibrium being shifted to a more associated ion pair. Moreover, this behavior could be ascribed to a directional interaction (i.e. H-bond) between the triazolium unit and the sulfonate anion (Scheme S4). The coordination pattern reported in Scheme S4 could also explain why new sets of resonances are visible at H_{Tr}^u and H_6^u (see Figures S31-S32). Conversely the chemical shift of H_{Tr}^c does not change appreciably, as expected for a fully dissociated ion pair. Our results show that two equivalents of camphorsulfonate are sufficient to afford a quantitative coordination of the unencircled triazolium station in CD_2Cl_2 at 223 K, and are in line with the stronger coordination ability of sulfonate in comparison with iodide.



Scheme S4. Hypothesized coordination pattern for the sulfonate anion binding to the uncomplexed triazolium station.

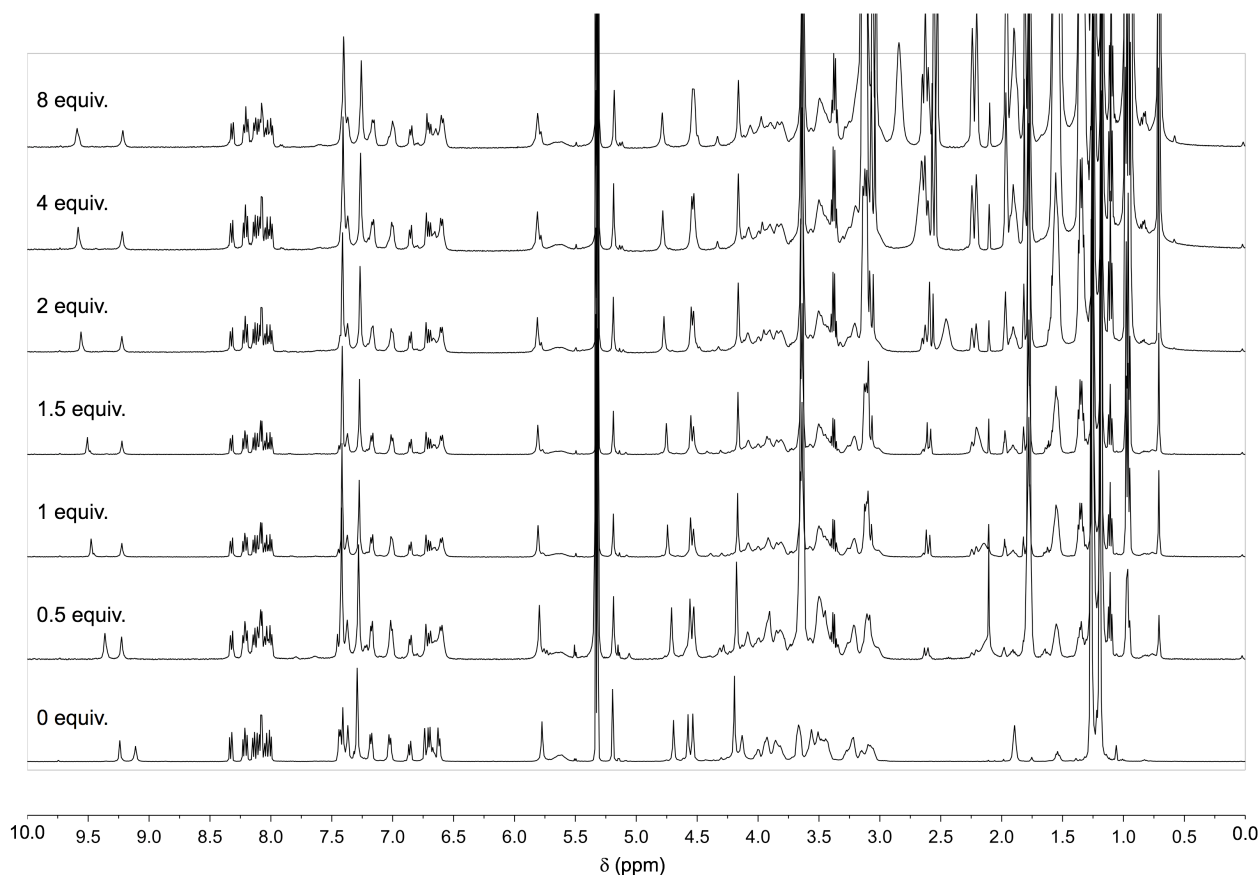


Figure S31. 1H NMR spectra (500 MHz, CD_2Cl_2 , 223 K) of $1^{2+} \cdot 2I^-$ (5 mM) recorded upon addition of 0.5, 1, 1.5, 2, 4, and 8 equivalents of TBA[(–)-CS].

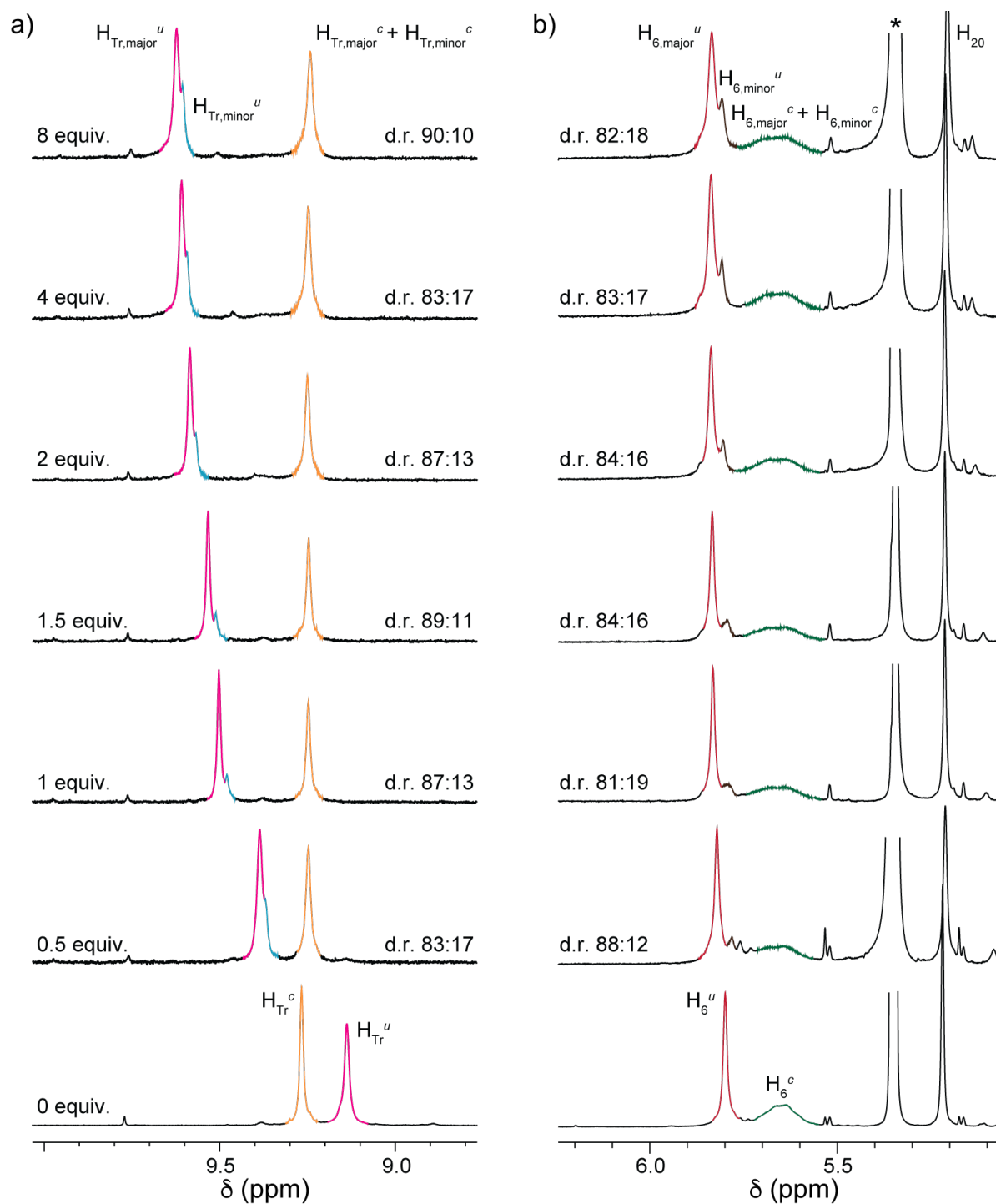


Figure S32. Partial ^1H NMR spectra (500 MHz, CD_2Cl_2 , 223 K) of $1^{2+}\cdot 2\text{I}^-$ (5 mM) recorded upon addition of 0.5, 1, 1.5, 2, 4, and 8 equivalents of TBA[(-)CS], showing the region of $\text{H}_{\text{Tr}}^{\text{u}}$ and $\text{H}_{\text{Tr}}^{\text{c}}$ (a) and that of H_6^{u} and H_6^{c} (b). The signal marked with an asterisk is the residual solvent peak.

4.8 ^1H NMR spectra of $1^{2+}\cdot 2\text{I}^-$ in the presence of Δ -TRISPHAT in toluene- d_8

^1H NMR spectra of 1^{2+} were recorded at 243 K prior and after addition of 8 equivalents of the tetrabutylammonium salt of Δ -TRISPHAT (TRISPHAT = [Tris(tetrachlorobenzenediolato) phosphate(V)]). Spectra recorded at temperatures below 243 K were poorly resolved due to precipitation. Deprotonation was performed in CD_2Cl_2 according to the protocol reported in section 4.1. The solvent was removed with a stream of argon and the residue was dissolved in 700 μL of toluene- d_8 (about 1% CD_3CN was added to improve the solubility).

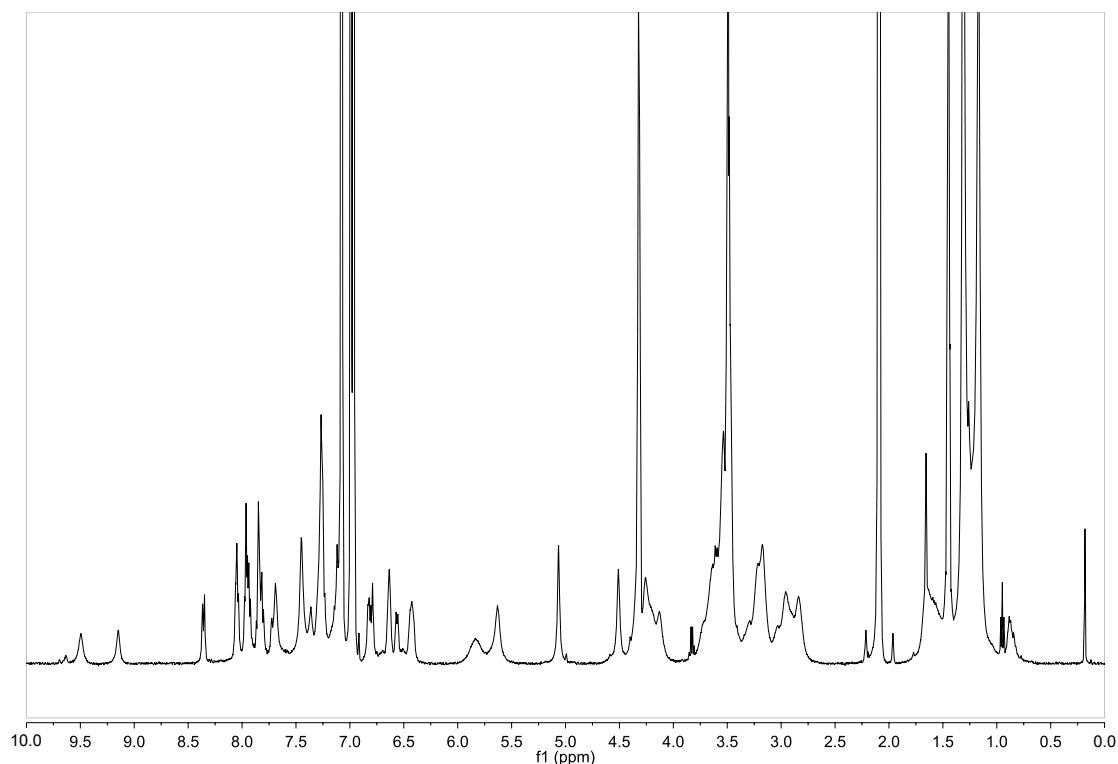


Figure S33. ^1H NMR spectrum of $1^{2+}\cdot 2\text{I}^-$ (500 MHz, toluene- d_8 , 243 K).

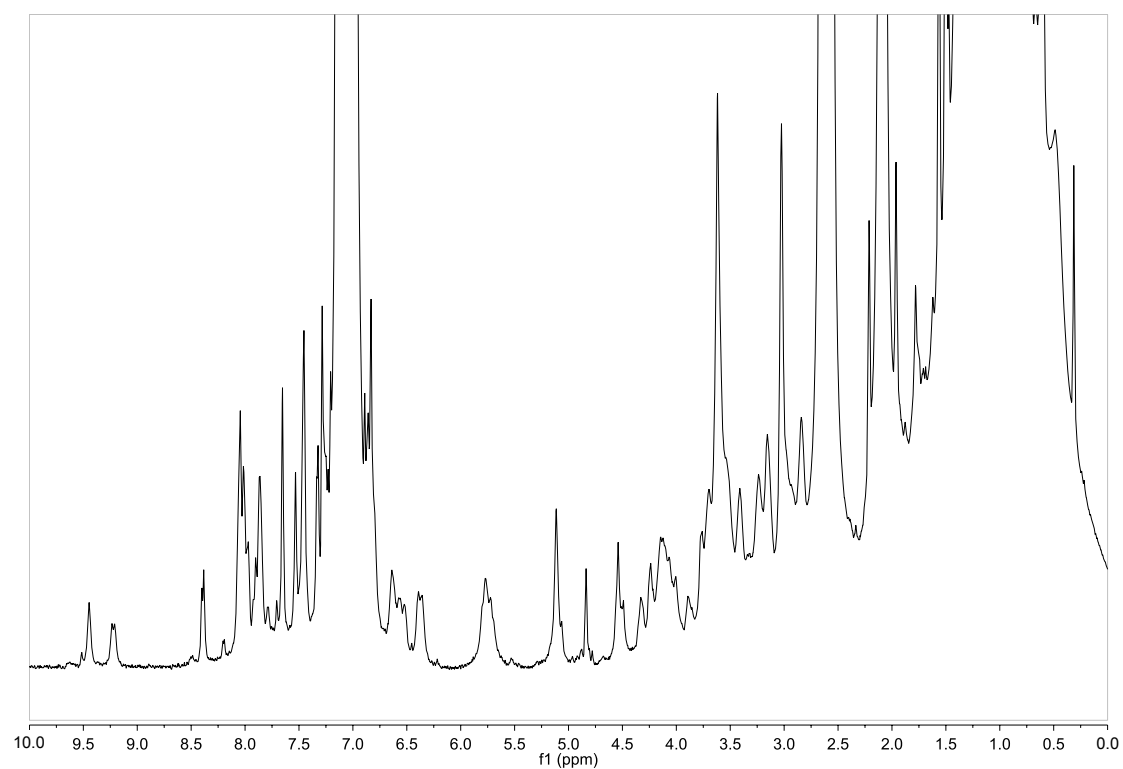


Figure S34. ^1H NMR spectrum of $1^{2+}\cdot 2\text{I}^-$ after addition of 8 equivalents of Δ -TRISPHAT (500 MHz, toluene- d_8 , 243 K).

5. Luminescence switching



Figure S35. Photographs under UV light (365 nm) of a 1.05×10^{-5} M solution of $1\text{H}^{3+} \cdot 3\text{I}^-$ (left) and $1^{2+} \cdot 2\text{I}^-$ (right), showing that the chemically triggered switching between the prochiral and the chiral states can be followed by the naked eye.

6. Circular dichroism

$1\text{H}^{3+} \cdot 3\text{I}^-$ was deprotonated according to the protocol reported in section 4.1. CD Spectra prior and after deprotonation do not show any features, as expected for an achiral molecule and a racemic mixture.

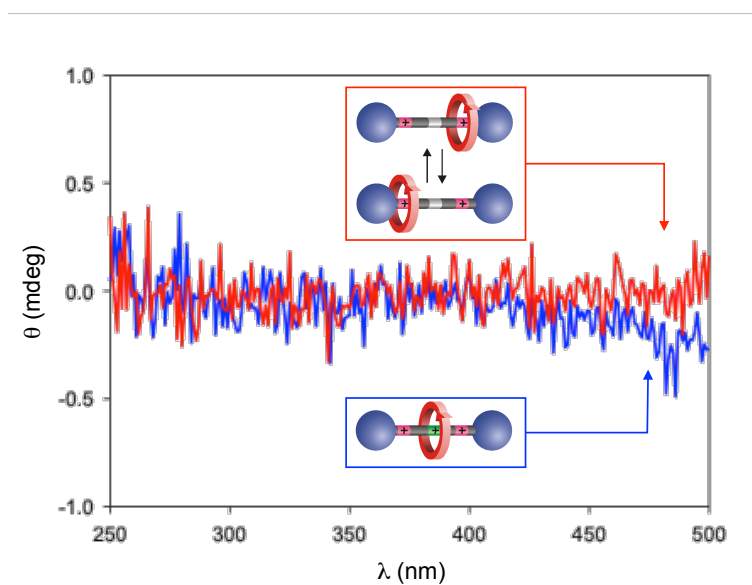


Figure S36. CD spectra of prochiral $1\text{H}^{3+} \cdot 3\text{I}^-$ (blue) and of racemic $1^{2+} \cdot 2\text{I}^-$ (red). Conditions: 1.05×10^{-5} M, CH_2Cl_2 , 298 K.

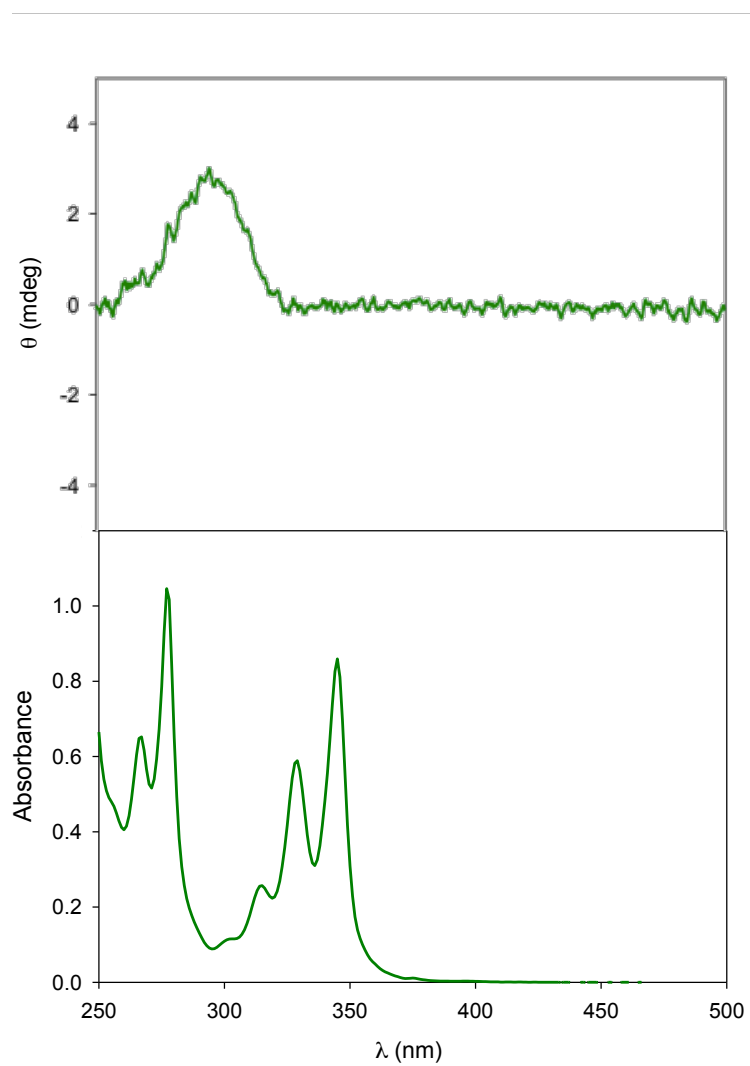


Figure S37. CD (top) and UV-Vis (bottom) spectra of $1^{2+} \cdot 2I^{-}$ after addition of 8 equivalents of [(+)-CS]. The CD band peaking at about 300 nm is due to the camphorsulfonate anion. Conditions: 2.6×10^{-4} M, CH_2Cl_2 , 298 K.

7. Molecular modelling

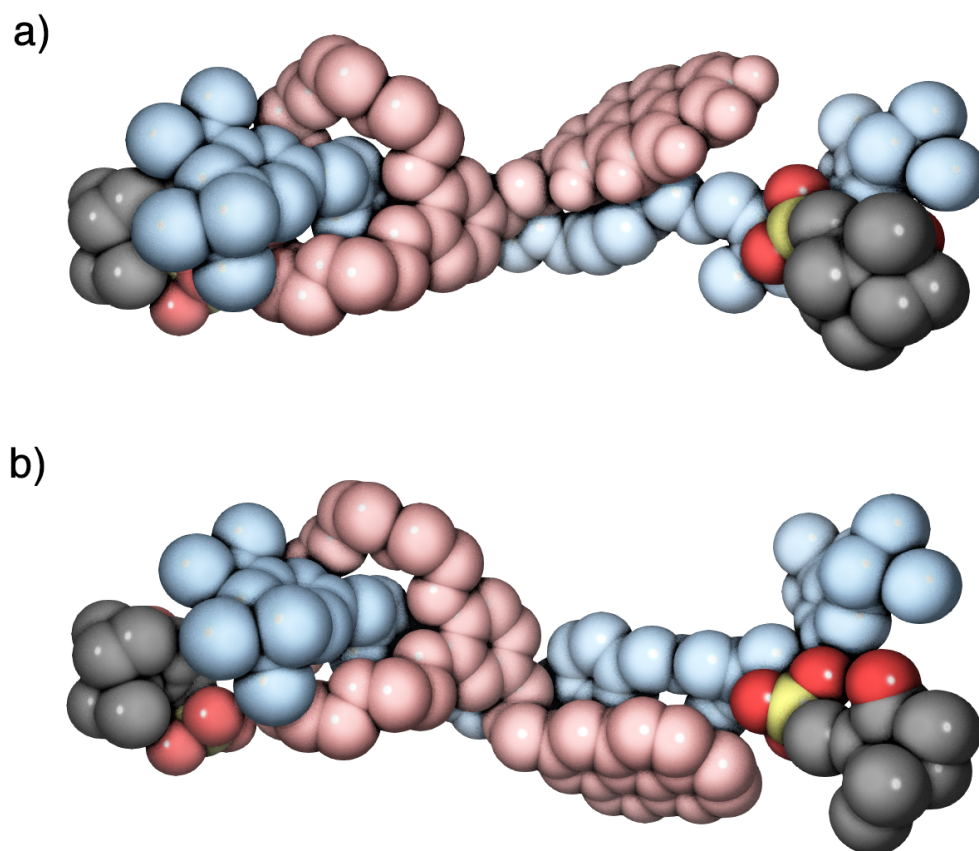


Figure S38. Molecular model (MacroModel 11.5, MMFFs force field) of the diastereomeric pair consisting of either (R_{mp})- 1^{2+} (a) or (S_{mp})- 1^{2+} (b) with one (-)-CS anion (on the right) coordinated to the unencircled triazolium unit. The triazolium unit encircled by the ring can only form a loose ion pair with another (-)-CS anion (on the left). Hydrogen atoms are omitted for clarity. It should be remarked that this modelling is not sufficiently accurate to provide physically realistic structures. The models are only meant to represent the proposed stereodifferentiation mechanism, which arises from the complexation between the chiral anion and the unencircled triazolium site in either enantiomeric co-conformation of the rotaxane.

8. References

- (1) Chatterjee, S.; Ramakrishnan, S. *Chem. Commun.* **2013**, *49*, 11041–11043.
- (2) Ragazzon, G.; Credi, A.; Colasson, B. *Chem. Eur. J.* **2017**, *23*, 2149–2156.
- (3) Schäfer, C.; Ragazzon, G.; Colasson, B.; La Rosa, M.; Silvi, S.; Credi, A. *ChemistryOpen* **2016**, *5*, 120–124.
- (4) Belowich, M. E.; Valente, C.; Smaldone, R. A.; Friedman, D. C.; Thiel, J.; Cronin, L.; Stoddart, J. F. *J. Am. Chem. Soc.* **2012**, *134*, 5243–5261.
- (5) Sommer, M.; Allain, M.; Mézière, C.; Pop, F.; Giffard, M. *Acta Cryst.* **2015**, *E71*, 748–751.
- (6) (a) Schulze, B.; Schubert, U. S. *Chem. Soc. Rev.* **2014**, *43*, 2522–2571. (b) Cai, J.; Sessler, J. L. *Chem. Soc. Rev.* **2014**, *43*, 6198–6213. (c) Busseron, E.; Romuald, C.; Coutrot, F. *Chem. Eur. J.* **2010**, *16*, 10062–10073.